POLITECNICO DI TORINO

Collegio di Ingegneria Chimica e dei Materiali

Corso di Laurea Magistrale in Ingegneria Chimica e dei Processi Sostenibili

Tesi di Laurea Magistrale

Sessione di Marzo 2025

CROSSLINKING, CHARACTERIZATION, SURFACE FUNCTIONALIZATION AND 3D-PRINTING OF AESO-BASED BIOPOLYMERS

Relatore:

prof. Marco Sangermano

Candidato:

Andrea Cocuzza

Contents

Dedication

To my family and friends, who supported me though trials and adversity

Abstract

This work aims to investigate the viability of acrylated epoxidized soybean oil-based crosslinked biopolymers, with the use different concentrations of glycidyl methacrylate as a co-monomer. Characterization of the liquid resin mixture and of the final polymer matrices were conducted to ascertain the physical properties of the material, resulting in a reliably crosslinked solid final product, with fast crosslinking and close to total conversion, and thermal-mechanical properties ranging between those of the two components. The prospective surface functionalization trials, aimed at the creation of a pH-sensitive fluorescent probe, revealed the intrinsic fluorescence of the material, which was determined to be nonspecific and invariable. The inclusion of the probe led to the conclusion that the intensity of emission by the probe decreases with the addition of solvents and acids, related respectively to the swelling of the matrix and protonation of the probe. Initial rheological analysis of the resin indicated that higher concentrations of GMA would be necessary for 3D printing, but attempts at producing artifacts with MSLA printing resulted in success even with resins containing low or absent concentrations of the co-monomer, as well as the capacity to produce complex features.

Acknowledgments

This work has been possible thanks to the joint efforts of Prof. Marco Sangermano, from Politecnico di Torino, and Dr. Paula Bosch from ICTP, in Madrid. Their support and expertise has been invaluable to the success of this nine month long project. I also wish to express my gratitude to every PhD and PhD student in Prof. Sangermano's team, with special regards to Alberto Cellai, Matteo Bergoglio, Dumitru Moraru and Matilde Porcarello and for coaching me through my first real research experience, as well as the great members of Dr. Bosch's group, with Maria Vittoria Piras and Natalia Cuesta Bañana aiding me and my work succeed in a new country.

Acronyms

AESO Acrylated Epoxidized Soybean Oil

GMA Glycidyl Methacrylate

GMA0 Formulation containing 0% GMA

GMA1 Formulation containing 1% GMA

GMA5 Formulation containing 5% GMA

GMA10 Formulation containing 10% GMA

BAPO (2,4,6-trimethylbenzoyl)-phosphine oxide (IRGACURE 819)

MCPBA meta-chloroperoxy benzoic acid

TFA trifluoroacetic acid

1. Introduction

1.1. Motivations

Plastics, and polymeric materials in general, are ubiquitous due to their ease of manufacturing, low cost, reliability, versatility, and unique physical and mechanical properties. Their use spans each and every industry, from packaging and consumer goods, to the tech field, construction, agriculture, all the way to cutting-edge pharmaceutical and medical applications.

Some of their main advantages, namely price and durability, come at a cost, that of environmental sustainability. In the present day, most commercially available plastic is economically advantageous to use due to its relatively cheap and widely available source materials, largely fossil fuels, whose supply is limited and unsustainable in the middle-to-long term. Similarly, its structural soundness and durability comes at the cost of biodegradability, since most of Earth's decomposer microbiome is unequipped to deal with such macromolecules. Nonetheless, not all uses of plastics require the materials to be indeterminately durable, and many solutions are being put forward to solve the problems of both bio-based monomers and biodegradability [1].

This work will aim to analyze the viability of *acrylated epoxidized soybean oil-*

based photopolymers, which have demonstrated promising properties in existing research, with the addition of glycidyl methacrylate as a reactive co-monomer, to increase the density of the functional groups of interest.

Furthermore, the possibility of adopting additive manufacturing (better known as 3D-Printing) as a mode of production was investigated, as it allows for a simple and cost-effective design phase of complex structures, compared to traditional methods, which often rely on complex and expensive externalities such as dies, molds and heavy machinery.

1.2. Free radical polymerization

Radical polymerization is one type of chain growth polymerization, meaning the growing polymer chain expands by one monomer unit at a time, rather than by doubling steps, causing a reaction that is fastest at the beginning, and slower towards the end. In free radical polymerization, the initiator is a radical species and the propagating center is a carbon radical, indicated by a bullet "•" sign associated to the atom that contains an unpaired electron each. Radicals are formed from compounds with symmetrical bonds (such as halogen molecules like Cl_2 or F_2) or molecules characterized by weak covalent bonds between groups with similar electronegativity. These bonds undergo homolytic breakage when supplied with sufficient energy, either from light, heat or chemical reactions, forming two groups containing an unpaired electron. These chemical species are highly reactive and they tend to quickly and easily propagate from molecule to molecule. The first reaction, known as an initiation reaction, forms the first radical species I•, which starts the chain reaction. In

photopolymerization, the initiator is a UV-sensitive compound which breaks down into radical species when exposed to light [2].

$$I_2 \xrightarrow{hv} 2I\bullet$$

Equation 1.1: Initiation reaction

The radical formed by the initiator, having a very low concentration, then goes on to react with one of the abundant monomer molecules surrounding it, forming a monomer radical M•, which in turn reacts with more unsaturated monomer molecules forming a growing chain P_n• that gets longer as long as monomer is available and free to diffuse in the growing matrix. Viscosity and its evolution are a crucial factor in determining the degree of polymerization, since the growing polymer chain cause the reagent mixture to thicken and eventually become solid, lowering the diffusivity of the monomer and possibly causing the formation of pockets of unreacted reagent. This issue can be mitigated by thoroughly mixing the reagent mixture, in order to disperse the initiator as finely as possible, and by keeping the material thin, which is most often the case in photopolymerization.

$$I\bullet + M \rightarrow I + M\bullet$$

$$M\bullet + M \rightarrow P_2\bullet$$

$$P_n\bullet + M \rightarrow P_{n+1}\bullet$$

Equation 1.2: Propagation reactions

Termination reactions occur when two radical species interact and their free electrons combine to form an electron pair, lowering the total amount of free radical present. Polymerization can be terminated by two mechanisms, the first being combination, in which two growing polymer chains $P_n\bullet$ and $P_m\bullet$ combine to form a longer molecule. The second mechanism is disproportionation, in which one chain scavenges a hydrogen atom from another, forming one saturated and one unsaturated stable chain. The termination rate increases as the concentration of radical species increases: this happens exclusively by virtue of the monomer content of the reagent mixture decreasing as it reacts with the growing chains, since the total number of radical species can only decrease after the initiator is exhausted. The prevalence of one termination mechanism over another depends on the nature of the monomer, disproportionation being the most prevalent for reactions between acrylate groups.

$$P_n \bullet + P_m \bullet \rightarrow P_{n+m}$$

$$P_n \bullet + P_{m+1} \bullet \rightarrow P_n + P_m = CH_2$$

Equation 1.3. Termination reactions

1.3. Vat photopolymerization technology

Vat 3D printing is a form of additive manufacturing in which a liquid mixture containing monomers, additives and a photoinitiator is selectively exposed to a light that triggers the initiation reaction, leading to the localized crosslinking of the polymer. Such techniques have several benefits compared to the more common fused filament fabrication (FFF), the most significant being a higher resolution and ability to render intricate details, given the small scale and precision of the incident light [3].

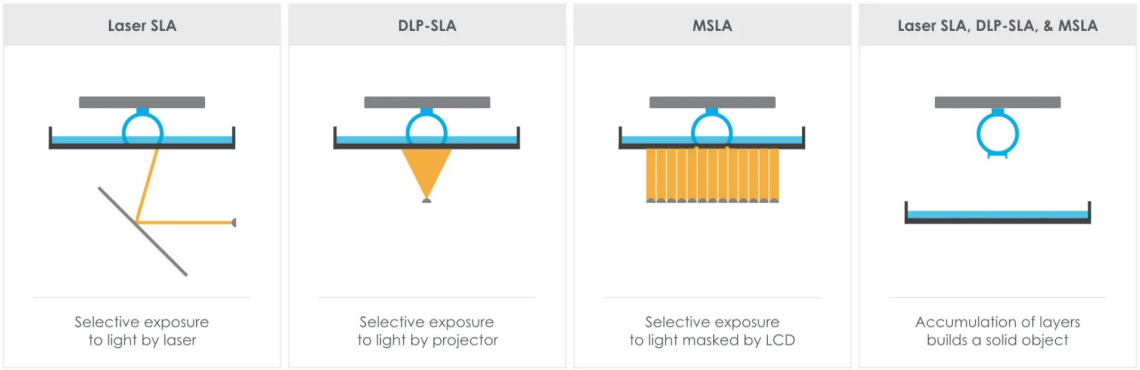

Figure 1.1: 3D printing technologies

In Stereolithography Apparatuses (SLA), a laser beam is focused on a path dictated by the *sliced* 3D model file in order to trigger a localized photochemical reac-

tion, inducing the crosslinking of the material in the desired area [4]. The vertical advancement of the building platform causes a new film of liquid resin to be exposed to the screen, allowing a new layer to be added to the print in progress. In SLA, XY resolution (a measure of the cross-sectional fidelity of the print) is determined by the laser spot size, and by the increments by which the laser beam can be controlled by the device. In the other foremost vat 3D printing technology, known as Digital Light Processing (DLP) devices on the other hand, an entire layer is projected the at the same time from a light-projecting display, through a series of micromirror devices, each representing a single 3D pixel (known as a voxel). DLP is thus limited by pixel size. The main advantage of SLA over DLP is the better resolution (as low as 25 μm, as opposed to 40-100 μm), at the cost of slower print speeds, since exposing the whole layer simultaneously is significantly faster than tracing the desired area [5].

Masked Stereolithography Apparatuses (MSLA) are based on a more recent technology, in which a light source is selectively masked in order to obtain the desired exposure. The development of this technique came about significantly later than SLA of DLP (both pioneered in the 1980s), as LCD screens capable of emitting light at 405 nm weren't available at the time. MSLA shares the weakness of DLP of being limited by pixel size, since lowering the pixel size in order to increase resolution (by increasing pixel density) lowers the overall optical density, increasing the necessary exposure time and thus negating the main benefit of DLP/MSLA. This inherent limitation is unfortunately linked to the intrinsic physical nature of LEDs, and thus difficult to overcome.

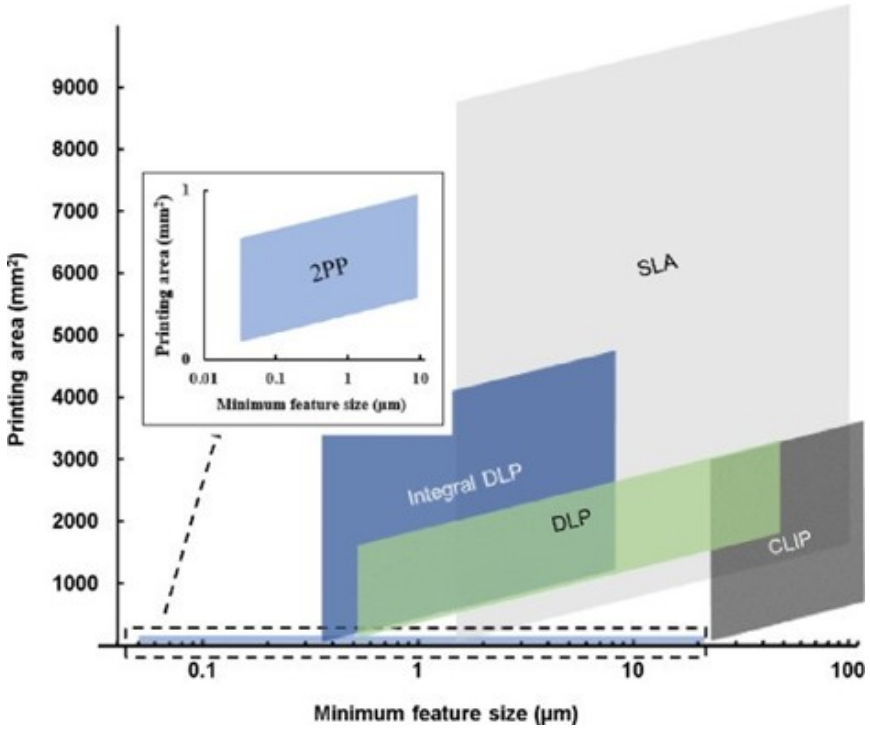

Figure 1.2: Technologies suitable for different feature sizes and printing areas

A crucial factor in determining the printability of a resin is the viscosity of the mixture. As mentioned previously, in any form of 3D printing, the advancement of the platform causes the partial print to detach from the projector screen, allowing the liquid to flood the area described by the previous layer. Since the resin needs to freely flow into this space, viscosity impacts the time required for complete saturation, and from it follows a crucial printing parameter, the delay between platform advancement and the start of the period of exposure of a new layer. A higher viscosity of the reagent mixture implies a longer delay, causing a significant increase in print time, meaning there is a limit to how viscous a resin can be while retaining commercial viability. Furthermore, the use of such resins increases the likelihood of poor layering, as well

as the formation of voids or defects.

1.4. Innovations in food packaging technology

Packaging materials account for 35-50% of the plastic produced worldwide, depending on what is considered as "packaging" and differing estimates [6], and food packaging is one of the main culprits for the abundance of single-use plastic, due to the necessity of a lightweight, inert material used in order to avoid contaminating the contents of the packaging: glass fails the former requirement, and aluminum the latter, while paper products fail when exposed to high humidity, which is most often the case in the food industry. Even containers made mostly out of other materials, such as aluminum cans or folding paperboard cartons, are almost without exception lined with a polymer coating in direct contact with the product, in order to provide a safe, inert layer to avoid leaching and scavenging between the container and its contents. The most widely used polymers for food packaging are low and high density polyethylene (HDPE/LDPE), polyethylene terephthalate (PET), polypropylene (PP), polystyrene (PS) and polyvinyl chloride (PVC) [7]. All these offer different characteristics, such as elasticity, mechanical resistance, permeability to different gases and liquids and chemical stability. They are also nearly irreplaceable in their own price range, as the production of oil-derived polymers is extremely cheap due to the low cost of the raw material and the scale of the global oil and gas market.

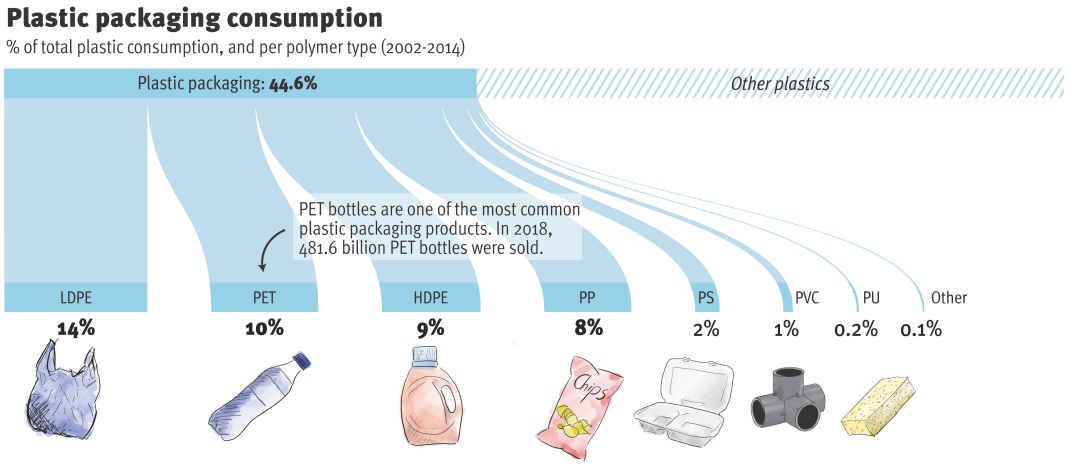

Figure 1.3: Plastic packaging as a percentage of global plastic consumption

Due to the widespread use and near inevitability of plastic in food packaging, it is crucial to avoid it whenever possible, and replace it with more sustainable alternatives when it isn't. Bio-based polymers such as those studied in this work offer a more environmentally friendly alternative to conventional plastics, especially in cases in which the mechanical resistance of the material is not the most crucial characteristic, such as the use cases discussed in this section.

In recent years, innovation in packaging technology expanded the field of *functional packaging*, a varied set of techniques that allow for better protection of the food, as well as communicating information and safety indications to the consumer [8]. Functional packaging can be subdivided into two categories: *active packaging* technologies involve the addition of new components either in the material itself, or in a separate body within its internal space, in order to release or absorb (scavenge) chemicals to improve the stability or the shelf life of the product, such as controlling humidity, gas composition, or the release of odors, plant hormones, or other spoilage

inducing substances, as well as release anti-microbial compounds.

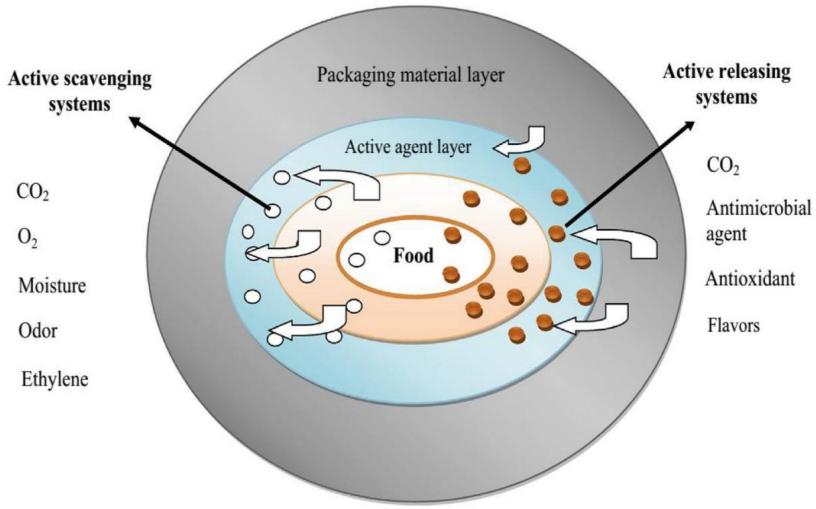

Figure 1.4: Active packaging technology

The second category, and the one of interest for this work, is *smart packaging*, and it involves communicating information to the operator and the consumer that couldn't otherwise be assessed with standard tools [8]. Such tools can be incorporated into the polymer matrix, or added onto the internal or external surface of the packaging, be it primary (such as bottles, tubs or trays), secondary (films or boxes containing the primary vessels), tertiary or quaternary (pallets and containers). These systems are varied in nature, one of the foremost factors in food safety being temperature, these range from limit temperature indicators, which trigger when an unsafe temperature is reached at any point of its life cycle, to integral temperature indicators which also factor time of exposure, using a product of time and temperature as a measure of exposure to unsafe conditions. Another relevant factor that can be monitored is the gas composition of the headspace of the container, such as

oxygen for oxidation, CO_2 and volatile organic compounds (VOC) for spoilage, or ethylene for vegetable ripening. Another crucial variable to monitor in food packaging is the pH of the contents, since plant matter releases volatile acids when it spoils, lowering the pH, while animal products rich in protein release ammonium compounds that raise it. Unaccounted for acidity can also be a sign of microbial growth, while alkaliphile bacteria are rare, especially in food. These indicators can be chemical, physical, enzymatic or biological in nature, and this work focuses on the former.

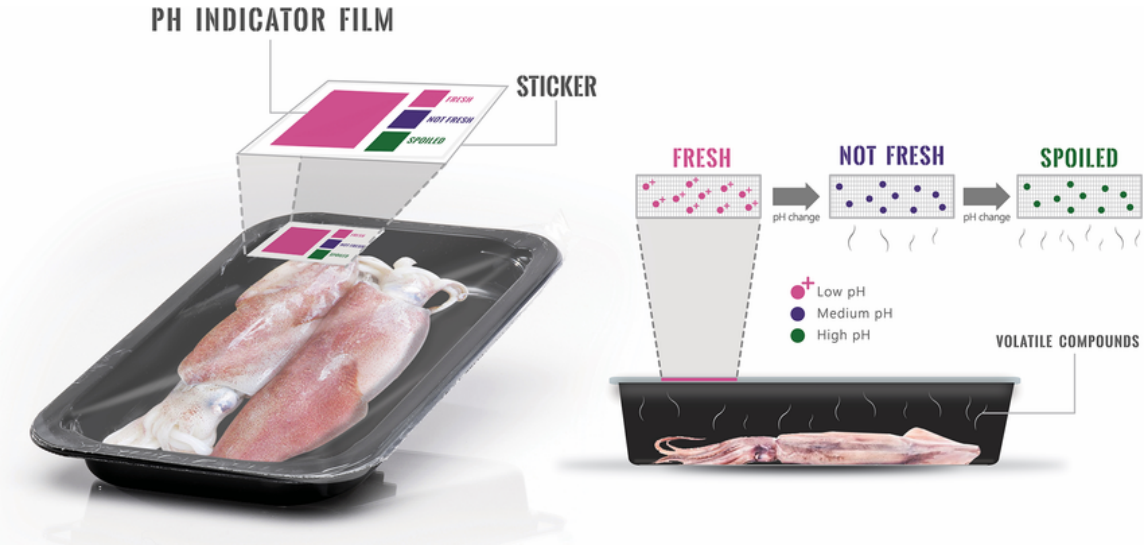

Figure 1.5: pH sensitive indicators

In this work, fluorescent compounds with pH sensitive luminescence were studied to determine their viability, both in acid solution and when exposed to volatile acids, when included in an acrylated epoxidized soybean oil (AESO) based matrix [9]. Such devices can be either included in the larger structure of a packaging unit, or applied to its inner surface via an adhesive polymer. This technology allows op-

erators and consumers to quickly assess whether a product has undergone unwanted alteration due to contamination or improper storage or handling, without the need to open and sample a package, allowing for a reduction of food waste and pathogenic contamination.

2. Materials and Methods

This section covers the experimental design and techniques used throughout the development and study of the properties of the reagent mixture and the final product, as well as the subsequent functionalization of the films.

2.1. Materials

The polymer is based on Acrylated Epoxidized Soybean Oil. Different formulations include different percentages of Glycidyl Methacrylate, used as a reactive co-monomer, given the greater density of the same reactive groups present in the main monomer, specifically epoxy and methacrylate groups. All formulations use (2,4,6-trimethylbenzoyl)-phosphine oxide (IRGACURE 819) as a photoinitiator. The *acronyms* section defines how these compounds are denominated henceforth.

2.1.1. Monomers

AESO is produced from soybean oil, one of the most widely available seed oils, characterized by a high degree of instauration [10]. The oil undergoes an epoxidation step (*Fig 2.1*) by a peroxycarboxyil acid such as MCPBA (meta-chloroperoxy benzoic acid), where a nucleophilic attack of the p-electrons belonging to the double bond by

the acid causes the formation of one C-O double bond, and the nucleophilic attack of the lone pair forms the other necessary for the cyclical epoxy structure [11]. Given that all vegetable oils only contain *cis* isomers, the final Epoxidized Soybean Oil (ESO) will be a pure enantiomer, since the reaction is *syn* stereospecific.

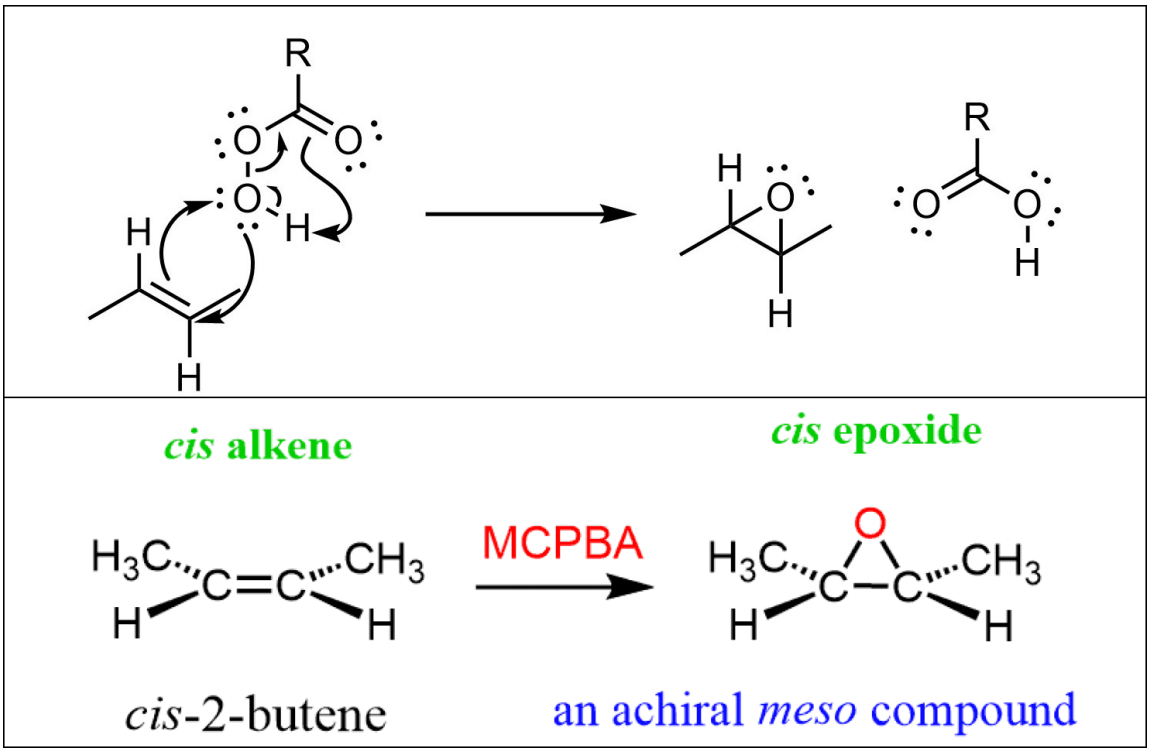

Figure 2.1: Epoxidation reaction mechanism

Following epoxidation, the resulting ESO undergoes an acrylation reaction (*Figure 2.3*), in which a certain number of epoxy groups react with acrylic acid to form acrylate groups. Acrylic acid can also be easily produced from most forms of biomass, including mono and polysaccharides, glycerol from lipids, and protein.

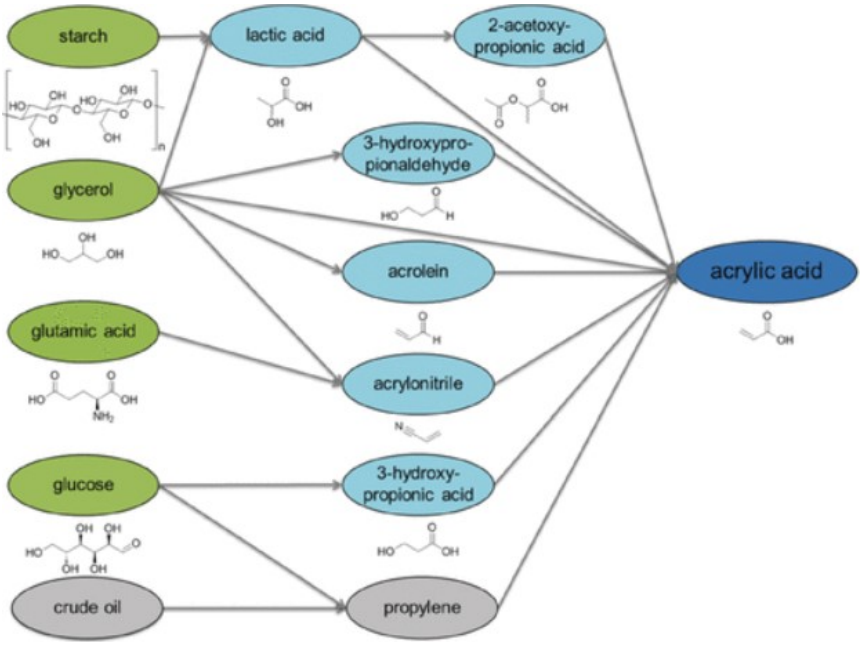

Figure 2.2: Sources of acrylic acid

The degree of acrylation, linked to the remaining concentration of epoxy groups, is a crucial design factor that must be accounted for and it can be used to tune the reactivity of the resulting product. This factor is highly dependent on the viscosity of the material, as the epoxidized oil becomes highly viscous. Because of this, viscosity control agents (VCAs) are often added in this step in order to lower the viscosity, which aids the completeness and homogeneity of the acrylation process.

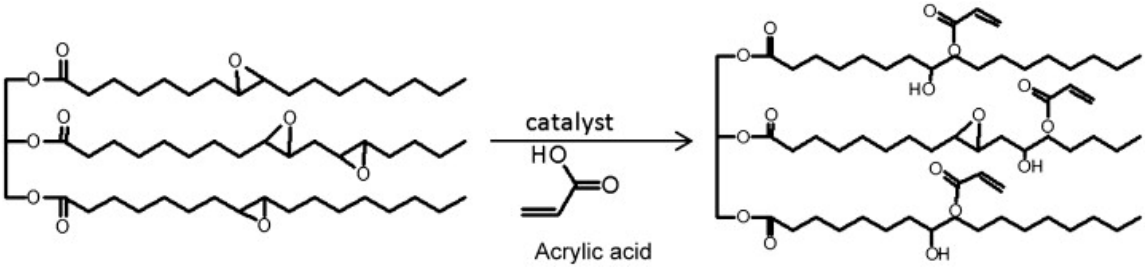

Figure 2.3: Acrylation of Epoxidized Soybean Oil

The co-monomer chosen for this study was Glycidyl Methacrylate, an ester of methacrylic acid and glycidol, a bi-functional molecule containing both an epoxide and a methacrylate group, widely used in photochemistry due to its high reactivity and action as a thinning agent. In this context, it provides both a way of reducing the viscosity of the reagent mixture, making it more suitable for 3D printing and generally easier to manipulate, as well as increasing the relative density of functional groups, enhancing the polymerization rate and producing a stronger material. Furthermore, the number of epoxy rings susceptible of further functionalization is increased in the obtained material.

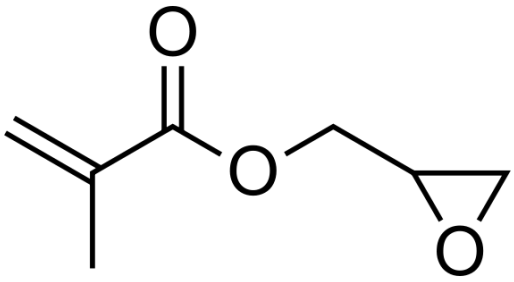

Figure 2.4: Glycidyl Methacrylate

2.1.2. Photoinitiator

The photoinitiator chosen for this work was (2,4,6-trimethylbenzoyl)-phosphine oxide, sold under the commercial name of IRGACURE 819, or BAPO.

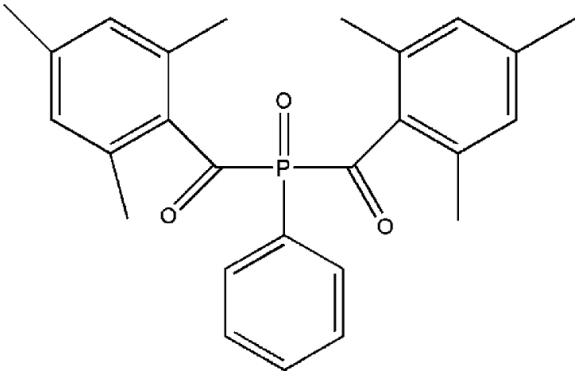

Figure 2.5: Chemical structure of BAPO

BAPO is a radical initiator commonly used in unsaturated resins for both surface and bulk applications. The reaction mechanism of initiation is displayed in *Figure 2.6* [12].

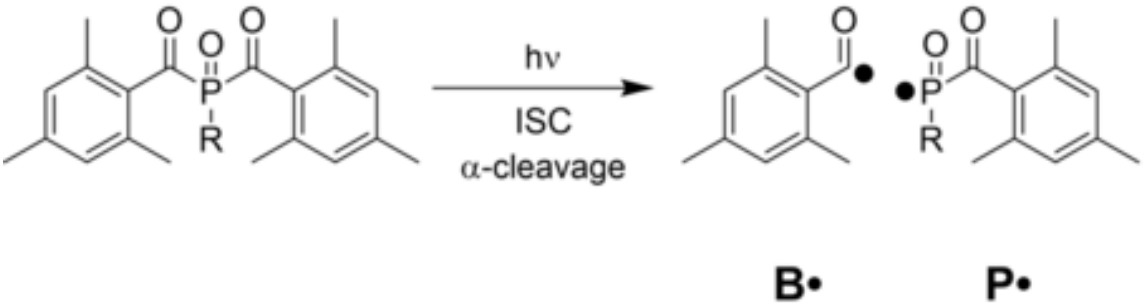

Figure 2.6: Initiation reaction

Exposure to UV light causes the homolytic cleavage of the phosphorus-carbon bond, due to its relative weakness and low difference in electronegativity between the two groups. The radicals formed by this reaction then go on to propagate the radical polymerization of the constituent monomers.

2.1.3. Formulations

Table 2.1 displays the contents of each formulation, as well as defining their names.

Formulations			
Identifier	AESO (wt%)	GMA (wt%)	BAPO (wt%)
GMA0	99%	-	1%
GMA1	98%	1%	1%
GMA5	94%	5%	1%
GMA10	89%	10%	1%

Table 2.1: Formulations

The different values of GMA content by weight were selected to provide a varied array of molar concentrations (discussed in *Section 3.3*). A low mass fraction of GMA corresponds to a significant value of molar concentration, given the much lower molecular weight of the co-monomer. This improves both the conversion of the resin (due to the higher concentration of functional groups) and the viscosity of the resin, which would have a negative impact on the 3D printing process.

2.2. Methods

The four formulations (GMA0, GMA1, GMA5, GMA10) were produced by adding the reagents in conical-bottom test tubes and placed in an ultrasonic bath at 50°C in order to thoroughly mix the monomers and allow the photoinitiator to dissolve. Whenever gas bubbles were found in the mixture in the following operations, a degassing step was conducted in the same apparatus. The tubes were wrapped in

aluminum foil to prevent accidental irradiation by ambient light (which could cause partial initiation of the polymerization reaction), and kept refrigerated at 4°C to avoid deterioration and evaporation of the GMA fraction, as indicated by the manufacturer. Before use, the reagents were left to heat up to room temperature, since AESO is extremely viscous and almost entirely unable to flow at lower temperatures.

2.2.1. FTIR spectroscopy

FTIR spectroscopy takes advantage of the specific interaction between molecules present in the sample and the infrared radiation striking it. Each type of molecular bond absorbs IR light at specific wavelengths, each corresponding to an energy level equal to the energy of the vibrational mode of the given bond. The instrument uses several iterations of recordings of absorption spectra with different combinations of multi-colored light, to retroactively compute a map of the values of absorption as a function of mirror displacement via the Fourier transform. The tool used to irradiate the samples was a *Hamamatsu LC8* xenon-mercury lamp, with a wavelength of 365 nm and an effective irradiance of 35 mW/cm^{-2}. The samples were progressively exposed to UV radiation in order to activate the photopolymerization reaction, recording the absorbance spectrum after each step. The degree of polymerization was analyzed by tracking the progressive decrease in intensity of the 810 cm^{-1} peak (measured as its area A_{peak}), corresponding to the acrylate group carbon double bond [13], with the sharp 1750 cm^{-1} ester C=O bond peak (A_{ref}) used as reference, since the area of the peak is a relative measurement rather than an absolute one. Such conversion η is calculated using *Equation 2.1*.

$$\eta = \frac{\frac{A_{peak}(t_0)}{A_{ref}} - \frac{A_{peak}(t)}{A_{ref}}}{\frac{A_{peak}(t_0)}{A_{ref}}}$$

Equation 2.1: Degree of polymerization

2.2.2. Photo-DSC analysis

Photo-DSC analysis was performed in order to further assess the reaction rate of each formulation when exposed to UV light. The test was performed on the *Mettler TOLEDO DSC-1* , with the addition of the UV lamp described in the previous section. The device operated at a constant temperature of 25°C, and samples with a weight of 3-5 mg were added to an aluminum crucible with a volume of 40 μL, under nitrogen atmosphere with a flow of 50 mL/min, with an empty crucible used as a blank reference.

Each run consisted of two steps: during the first, the sample and reference are both irradiated with UV light at a constant temperature until the sample is fully cured. In the second, the already cured sample and the reference are irradiated for a second time for the same duration and at the same temperature. Finally, the difference between the first and the second irradiation is calculated (via curve subtraction) to determine the pure heat of reaction. This allows for a detailed thermal analysis purely of the curing process, by discounting the effect caused by the irradiation itself. This process yields a specific enthalpy [W/g] as a function of time [s] curve, whose peak h_p is proportional to the specific heat of reaction, and thus the reaction rate.

The time-to-peak (t_p) constitutes the time to reach the maximum reaction rate.

2.2.3. DMT analysis

Dynamic mechanical thermal analysis was used to characterize the mechanical properties of the polymer over a range of temperatures, specifically the evolution of the *storage modulus* E' and *loss modulus* E", which characterize respectively the elastic and viscous deformation of the material. The analysis is conducted by cooling down the sample and its environment via liquid nitrogen, followed by cyclical applications of uniaxial tension on the ends of the material with a frequency of 1 Hz, while heating the instrument at a constant rate of 3°C/min. The ratio between the two moduli is known as the *loss* or *damping factor* $\tan(\delta)$ and the abscissa of its peak corresponds to the glass transition temperature of the material. The value of E' at the plateau was further used to determine the crosslink density of the cured matrix. The initial and final temperatures of -10°C and 110°C were chosen to yield a clear picture of the glass transition and to reach the ultimate rubber plateau, while the heating rate must be slow enough to yield a detailed curve.

2.2.4. Rheology

The rheological properties of the reagent mixture were studied in order to verify whether the viscosity of each mixture fell within appropriate limits for the purpose of 3D printing. Anecdotally, they appear significantly viscous and thus difficult to handle at room temperature, with a lower viscosity as the GMA content increases. Measurements were performed at a constant frequency of 1 Hz and at a constant

temperature of 25°C, with the two 25 mm wide plates set up at a distance of 1 mm. The rheometer was set to analyze the sample at a shear rate varying between γ'=0.01-1000 s^{-1}. The desired target for vat photopolymerization is a value of viscosity between η=0.2-10 Pa*s for shear rates at around γ'=1-10 s^{-1}, within the test parameters. Higher viscosities could lead to poor layering, voids and defects resulting from insufficient flow of the material as the print advances. This can be solved by slowing the advancement rate of the print, but such a solution may lead to a dramatic increase of the print time.

2.2.5. Photorheology

The photorheological analysis of the samples was conducted on the same instrument as the rheological, while exposing the material to a UV light at conditions equal to those used for the FTIR analysis as well as the conventional curing method described in *Section 2.2.6*. The device was set up with the same upper plate described in *Section 2.2.5*, with the addition of a 30 mW/cm^2 light source, and replacing the lower plate with a transparent one in order to allow the light to shine through it and cause the polymerization of the material. Furthermore, the distance between the plates was increased to 3 mm. The samples were held in the device for 60 s before initiating the irradiation to ensure homogeneity and to consolidate the results of the rheological analysis.

The aim of this trial is to essay how the viscosity of the monomer-polymer mixture develops as it crosslinks, in order to identify the gelation time of the curing sample, defined as the time needed to reach the inflection point in the viscosity over time

curve [14].

2.2.6. Swelling behavior

The swelling behavior of the material was analyzed in order to verify the structural soundness of the polymer when exposed to different solvents, namely water, ethanol and acetonitrile. These experiments were conducted via gravimetric measurement at increasingly higher time intervals until a plateau was reached for the mass measurement, assuming the value at the plateau as the final degree of swelling. After such procedure, the samples were left to dry in a well ventilated area to verify whether the de-swelling left the material brittle or damaged. This is relevant towards several possible techniques that can be used to functionalize the polymer, most of which involve immersion in an organic solvent.

2.2.7. Mold production and usage

One of the avenues explored to produce the polymer samples is via silicon molds, alongside 3D printing, according to the results described in *Section 3.1.* The sample dimensions were selected in order to fit diagonally in a 1*1 cm cuvette that would be used for the fluorimeter measurements, meaning 1.3*4 cm, with a thickness of around 0.8 mm in order to minimize cupping and warping. This choice is further discussed in *Section 3.6.*

The molds used to create the samples were cast in silicone over a 3D printed negative, for ease of production. These negatives were modeled and fabricated similarly to the 3D printed samples and produced using commercial resin, since they need to

be rigid and durable.

The molds were then filled with the reagent mixture and allowed to settle to get rid of any air bubbles, in order to avoid empty spaces in the final product. The full molds were subsequently cured under a UV light source, under a containment dome constantly flushed with nitrogen glass, a necessary precaution to avoid the inhibiting effect oxygen causes on the cross-linking of acrylate and methacrylate groups. The exposure time was selected according to the results of the FTIR analysis described in *Section 3.1.*

2.2.8. Superficial inclusion of the pH-sensitive probe

The aim of this study was to evaluate the possibility of functionalizing the surface of the material, taking advantage of unreacted epoxy groups within the polymer matrix in order to bind it with a pH sensitive fluorescent probe [15]. Further investigation proved that the probe could be included by immersion in the solvent-probe solution. This allows the solution to diffuse into the surface layers of the samples, which causes the probe to be included into the samples, and as the solvent evaporates after the samples are taken out of the solution, the probe is left behind in the matrix. The probe, by the name of nBu-NAP-EtOH (pictured in *Figure 2.7*), was synthesized and purified to a desirable degree, and it reacted as predicted to acid additions in solution, increasing its fluorescence as the pH of the solution decreased. The naphthalimide core of the molecule constitutes the fluorophore, while the free electron pair on the nitrogen is free to interact with acid, increasing the intensity of the fluorescence, which allows for its use as a pH-sensitive probe.

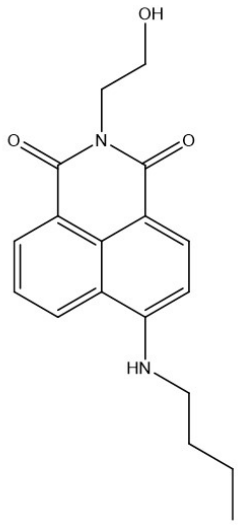

Figure 2.7: 4-(N-butylamino)-N-(2-hydroxyethyl)-1,8-naphthalimide

Initial testing indicated that the swelling of the matrix within a solution containing the probe, followed by a thermal treatment meant to bind the free probe to the polymer, would be the most straight-forward method of obtaining a functionalized matrix, which sparked the study of the swelling behavior of the material previously discussed.

Preliminary fluorimeter measurements of the swelled, but not yet thermally treated matrix were taken in order to verify that the probe did, in fact, diffuse into the polymer matrix as the material swelled. However, as described in *section 3.7*, the reading associated to the swelled matrix resulted too strong by several orders of magnitude compared to the reading of the probe in solution, which couldn't be explained by the contribution of the probe by itself. Furthermore, gathering such data required activating the attenuator built into the device, which lowered the signal by 99% in order to bring it down to the range of the device. This requirement further dimin-

ished the quality of the reading, as the attenuated signal has an intrinsically lower resolution compared to the original one. The intensity of the intrinsic fluorescence of the material was determined to be nonspecific and invariable over the region of the probe fluorescence.

Because of this, the matrix by itself, without addition of the probe, was tested for intrinsic fluorescence, resulting in a confirmation that the material was indeed fluorescent enough to interfere with the signal emitted by the probe, obscuring it by virtue of being several orders of magnitude stronger. These results, discussed in the aforementioned section, informed a further study of the exact dynamic of the intrinsic fluorescence of the matrix, which appeared to vary significantly when exposed to a solvent, as well as changes to the pH of the solution. The decrease in fluorescence was measured on the naphthalimide band.

Due to this unexpected outcome, the samples were tested for the development of their intrinsic fluorescence over time while immersed in water, acetonitrile, pentane and ethanol, followed by the addition of small amounts of trifluoroacetic acid (TFA) to lower the pH. Additions of liquid acetic acid were used to test the reaction of the sample to gaseous acids in dry conditions.

2.2.9. Fluorescence measurements

Fluorescence spectra were recorded on a Perkin–Elmer LS-55 spectrofluorimeter. Excitation wavelength (λ_{ex}=440 nm) was selected at the maximum absorption of the fluorescence probe in the matrix. The samples were obtained in a strip geometry of 3*1.3 cm and placed diagonally in a 1*1 cm cuvette. For the experiments conducted

under immersion, the cuvette containing the sample was filled with acetonitrile and inserted into the fluorimeter, which was programmed to take measurements of the intensity of the signal at periodic intervals, in order to monitor its development. After a set time, 50 μL of TFA were added to test the effect of the protonation of the matrix-probe complex. Similar experiments were conducted in dry conditions, by adding 50 μL of acetic acid to the bottom of the cuvette containing the sample but no solvent and leaving the acid to evaporate.

2.2.10. MSLA 3D printing

The 3D printer used to fabricate the samples is a *Phrozen Sonic Mighty 4K* alongside a *Curing Station* by the same brand. The printer is equipped with a LED light source emitting at λ=405 nm and uses the MSLA logic described in *section 1.2*.

The parameters selected for the print were 25 μm thickness and 8 s of exposure for each layer, rather standard for MSLA, and a significant 13 s delay between layers to account for the higher than average viscosity of the resin.

One of the main advantages of 3D printing is allowing the creation of more complex structures that would be excessively time and resource intensive to render into molds, which opens up the possibility of creating complex shapes with high specific surface, that retain a high exposed area while minimizing the volume, and thus the material cost of the part. Due to this, more complex structures were selected in order to essay the capacity of the resin to form harder to shape parts, such as joints, overhangs and empty spaces.

The first structure of choice to test the resin was a repeating hollow honeycomb

mesh constructed out of hexagons 2.5 mm to a side, with a width of 0.5 mm, and a height of 5 mm. Given the repeating structure, each cross-sectional part of the print ends up being 1 mm wide, from two hexagons touching. The outer walls were offset by 0.5 mm to account for the absence of the hexagon on the other side.

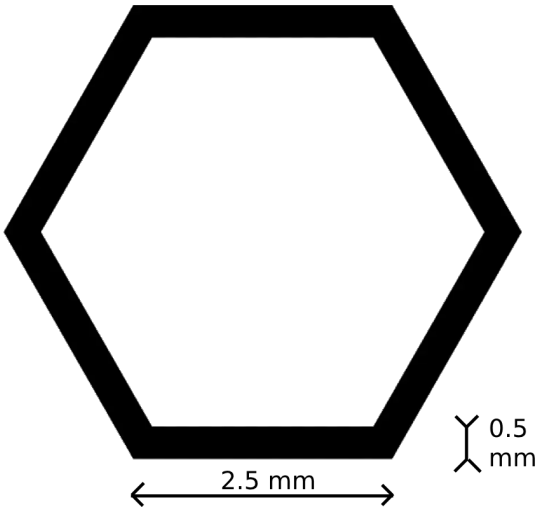

Figure 2.8: Honeycomb cell

Honeycomb structures are relevant in many fields of application of materials engineering, since they react better than square meshes to tangential forces, since they are spread over a larger area due to the 120° angle between each section, as well as offering excellent rigidity to perpendicular forces with minimal material expenditure, which also significantly reduces weight. Such structure are also indicative of the ability of the resin to form smaller features and sharp corners, which can be a challenge for the lesser performing formulations.

The last group of structures chosen to test the resin were selected among a wide category of solids known as *triply periodic minimal surfaces*. The concept of minimal

surfaces arose from the analysis of the physical interfaces between fluids, since they tend to stretch and distort indefinitely in order to achieve an energy minimum, which for immiscible fluids (including air) is the least possible surface area. All minimal surfaces share the characteristic of a mean curvature of zero. A minimal surface locally minimizes its total surface area given a certain set of constraints, such as one or more perimeters, a given volume to segregate, or minimal potential energy.

These structures also offer a good chance to test some of the most challenging aspects of 3D printing, largely revolving around unsupported horizontal features. Most minimal surfaces contain one or more of these complex parts, such as voids and overhangs, which can cause a print to fail entirely by either layer detachment or structural collapse, as well as smooth, low curvature inclines, which can strongly highlight poor layering and fraying of the edge of the artifact. Being able to print these notoriously complex features is one of the hallmarks of a reliable resin.

The minimal surface structures chosen for this work were the Fisher-Koch S structure, the Schoen F-RD structure and the gyroid.

Fisher-Koch S structures are composed of two interwoven, non-intersecting volumes and they are commonly used in thermal exchange applications, because they feature a high surface to volume ratio and null surface curvature typical of minimal surfaces, while retaining sufficient mechanical resistance [16]. The two separate channels allow for complete segregation of the fluids undergoing thermal exchange.

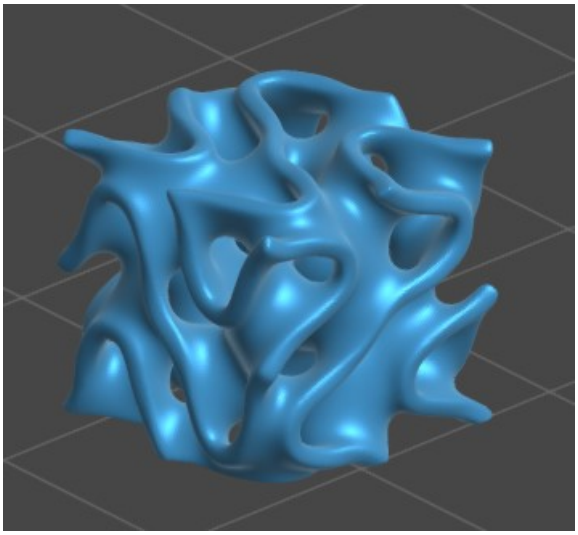

Figure 2.9: Fisher-Koch S structure

Schoen F-RD structures [17] arise from the study of face center cubic lattice structures, and they are relevant for sphere-packing problems. They possess tetrahedral symmetry.

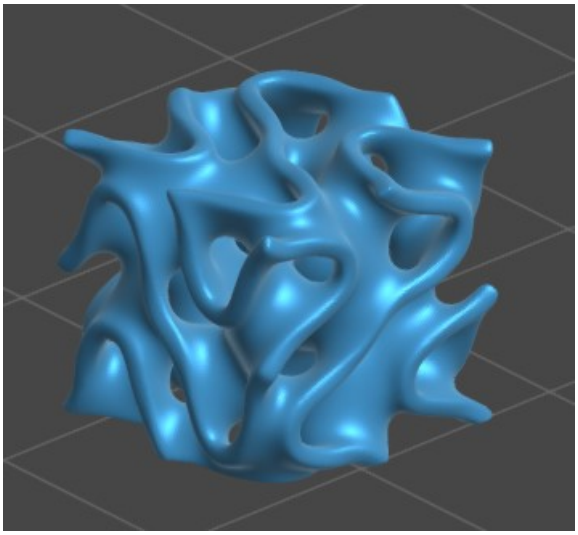

Figure 2.10: Schoen F-RD structure

Gyroids are the most well known minimal surface solids and they often constitute a model structure for the behavior of a material. These structures segregate two separate channels and they possess no straight lines or planar symmetries. Gyroids have been observed as naturally forming structures in biological polymers, and they are one of the smallest mechanically stable 3D structures [18].

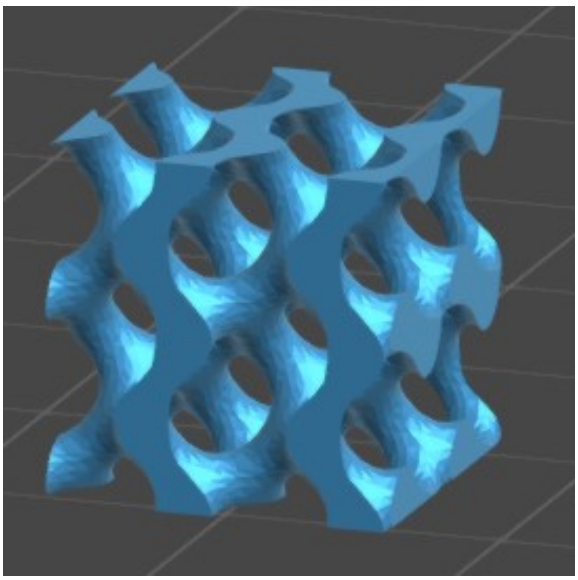

Figure 2.11: Gyroid structure

The totality of these five models includes a wide range of complex features, resulting in a thorough characterization of the ability of each resin to render 3D artifacts with precision.

3. Results and Discussion

The aim of this section is to depict a thorough description of the material, both the reagent mixture and the final polymer, as well as its functionalized form. Furthermore, possible applications and future research paths are discussed.

3.1. FTIR spectroscopy

FTIR spectroscopy was used to investigate the evolution of degree of polymerization at different exposure intervals, in order to define the polymerization parameters.

Figure 3.1 displays an example of the evolution of the relative intensity of the 810 cm^{-1} peak, corresponding to the acrylate group carbon double bond, for the GMA10 formulation.

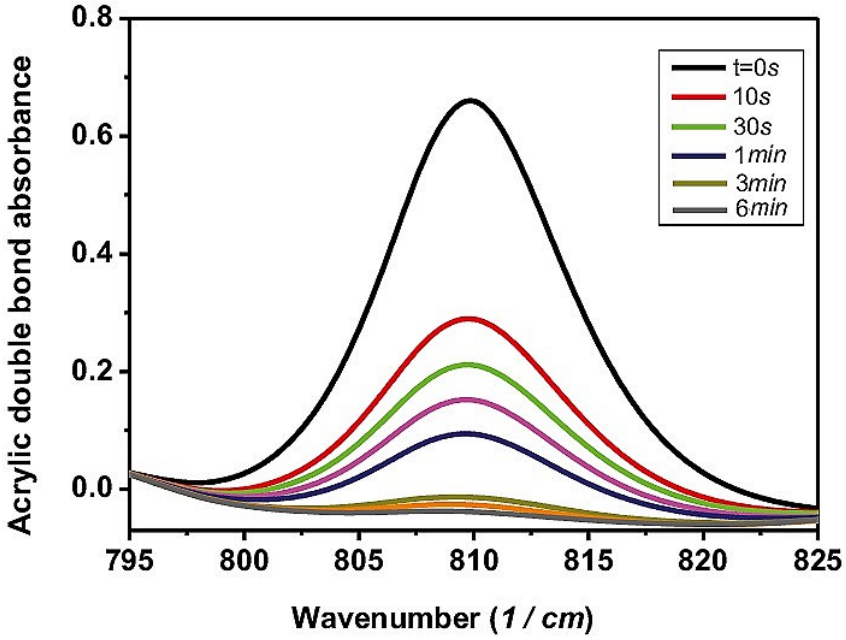

Figure 3.1: 810 cm^{-1} relative peak intensity over time

Figure 3.2 shows how the conversion of the monomer mixture (defined as the percent variation of intensity of the 810 cm^{-1} peak) develops over time, with increasing UV exposure.

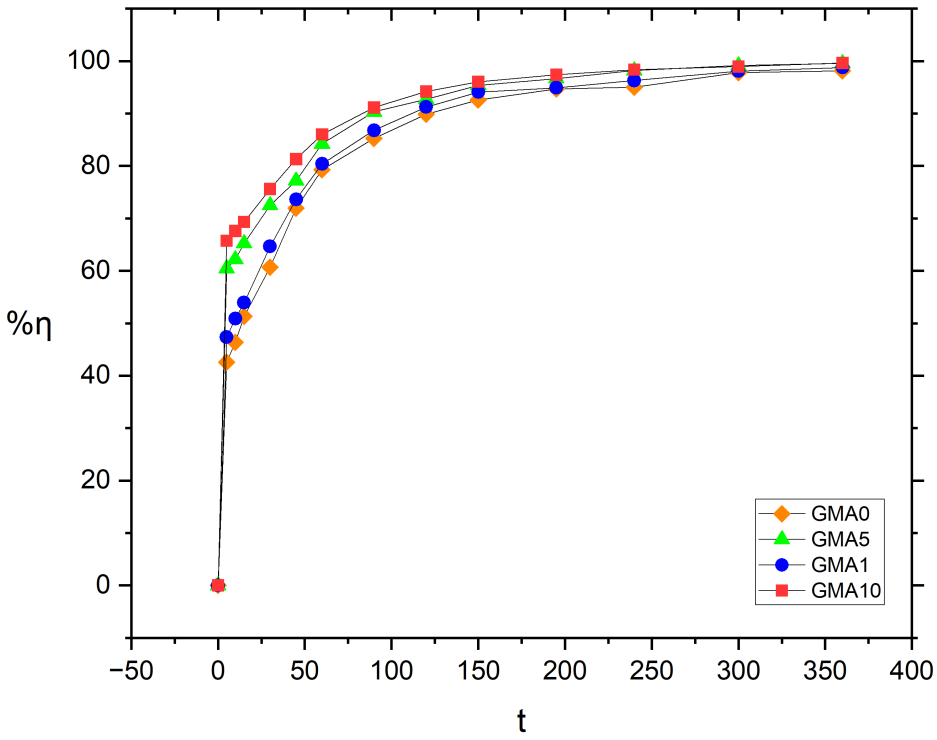

Figure 3.2: Conversion rate by FT-IR analysis

Formulations with a lower GMA content demonstrate a significantly lower reaction rate, especially at lower exposure times, indicating that the co-monomer has a favorable effect on kinetics, given the higher concentration of reactive groups. For reference, this causes a 17.98% difference in conversion between GMA0 and GMA10 at 15 seconds. On the other hand, the difference in ultimate conversion (at t=6 min exposure time) is only slightly influenced by the nature of the formulation, with only a 1.48% difference.

Both the reaction rate and ultimate conversion were likely impacted by the envi-

ronment the trials were conducted in, as the polymerization of acrylates is inhibited by oxygen, and the device used for the analysis couldn't be flushed with nitrogen in order to displace the oxygen. Because of this, the times and reaction rates derived from these results can be understood as a lower bound to the real crosslinking properties of the material.

The results indicate that the polymerization reaction proceeds quickly for all four formulations, and this fact is corroborated by trial samples being able to hold their shape after thirty seconds of exposure for the GMA0 and GMA1 formulations, and only twenty seconds for GMA5 and GMA10. In order to thoroughly convert the reagents, a total exposure time of five minutes was selected, comprised of three minutes for one side, and two minutes for the other. This is significantly higher than the time strictly required to obtain a structurally sound material, but further processing of the polymer requires immersion in organic solvents, and such long exposure time minimizes the leaching of unreacted monomer in the solution.

3.2. Photo-DSC analysis

Time-dependent specific heat flow curves of all formulations are shown for each formulation in *Figure 3.3* and the results are summarized in *Table 3.1.* ΔH represents the integral of the specific heat flow recorded from the sample, while h_{peak} and t_{peak} are respectively the height of the peak and the time the sample required to reach it.

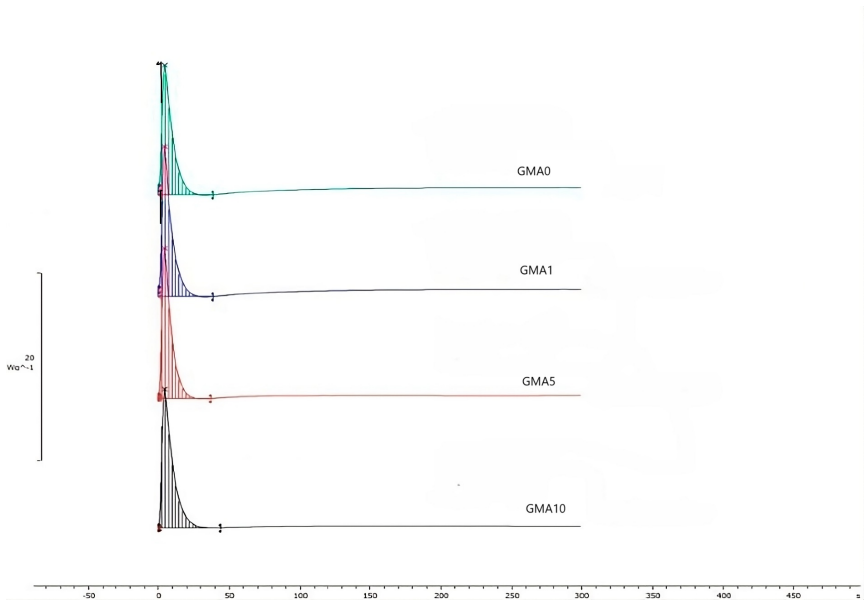

Figure 3.3: Specific heat flow over time

Formulation	ΔH [J/s]	h_{peak} [W/s]	t_{peak} [s]
GMA0	136.6	13.23	3
GMA1	138.4	12.96	3
GMA5	141.9	14.61	3
GMA10	145.0	14.83	3

Table 3.1. Thermal properties of each formulation

The results show a small difference in the heat of reactions, which increases both in total magnitude and maximum intensity as the concentration of GMA increases. These results are in agreement with previous findings from FTIR analysis, and they don't represent a meaningful difference regarding the choice of formulation for significant applications.

3.3. DMTA characterization

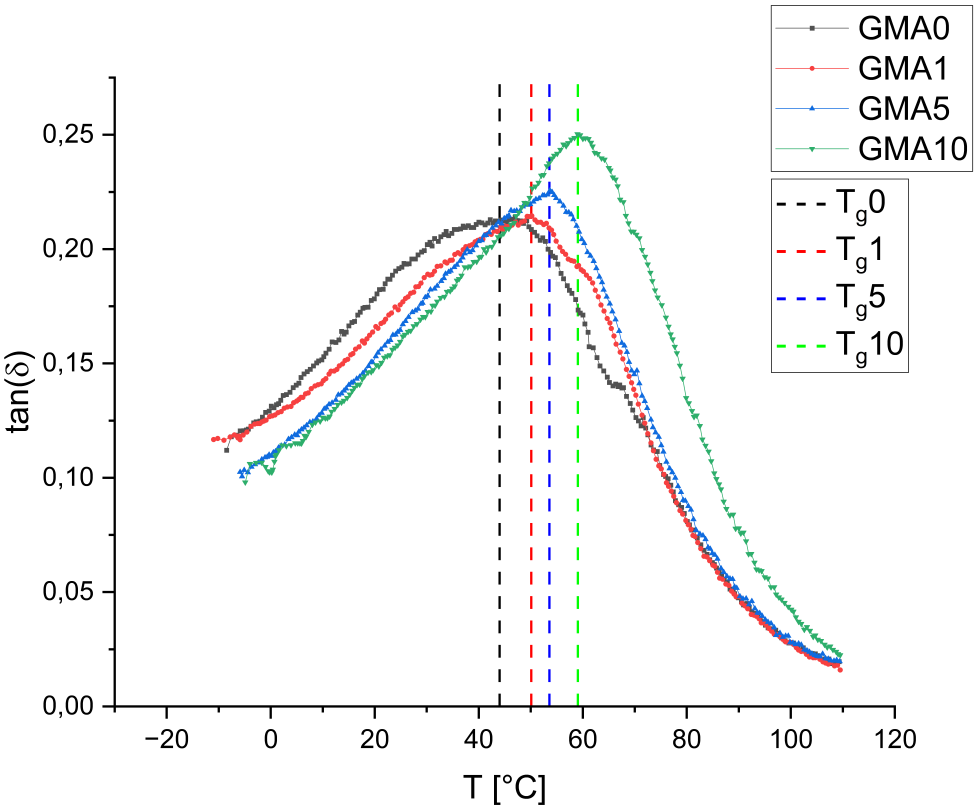

Figure 3.4: Glass transition as the temperature at peak of tan(δ)

Figure 3.3 displays the value of tan(δ) as a function of temperature, in a range (T= -10∼110°C) sufficient to describe the glass transition and ultimate rubber plateau behavior of the material, at a frequency of 1 Hz.

Formulation	GMA Molar concentration	T_g
GMA0	-	49.3°C
GMA1	0.0786	51.4°C
GMA5	0.3078	55.7°C
GMA10	0.4842	59.4°C

Table 3.2. Glass transition temperatures T_g

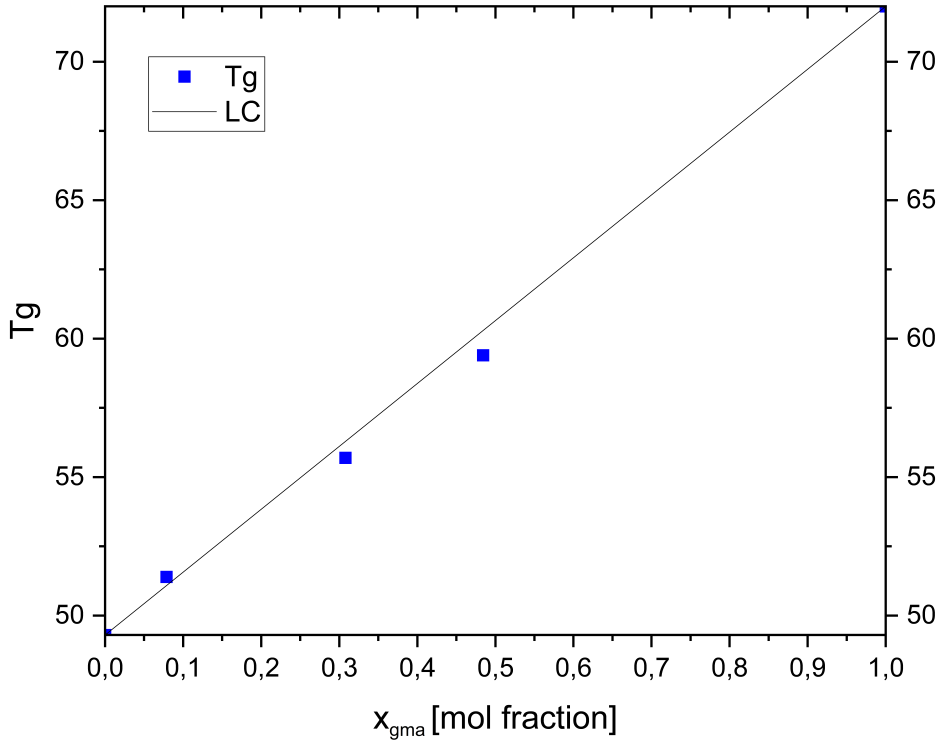

Figure 3.5: Glass transition temperature as a function of GMA concentration

The results are summarized in *Table 3.2.* and rendered into *Figure 3.5.* Given that the polymer based on pure AESO (corresponding to the GMA0 formulation) displays a T_g=49°C and considering a T_g=72°C for pure poly(glycidyl methacrylate) [19], these results fall within expected values.

"LC" represents an ideal linear correlation, described by *Equation 3.2*, between the molar concentration of GMA (calculated via *Equation 3.1.* from its weight fraction and considering a molecular weight of 1200 g/mol for AESO given by the manufacturer) and the recorded glass transition temperature [20]. The correlation is drawn between the aforementioned T_g of the pure monomers. The data points recorded in the experiments display that the linear model is applicable to this specific comonomer, as expected for mono-substituted monomers from relevant literature.

$$x_A = \frac{\frac{w_A}{M_A}}{\frac{w_A}{M_A} - \frac{1-w_A}{M_B}}$$

Equation 3.1: Molar fraction

$$T_g = x_a T_a + x_b T_b$$

Equation 3.2: Ideal linear correlation

$$v_c = \frac{E'_{ult}}{3RT}$$

Equation 3.3: Crosslink density

The ultimate value of the storage modulus E' for each formulation was used to determine the volumetric density of crosslinks by using *Equation 3.3*, E'_{ult} being the value of E' at T* = T_g + 50°C.

Figure 3.6 displays the development of E'(T*) and *Table 3.2* its ultimate value for each formulation, as well as the calculated value of v_c.

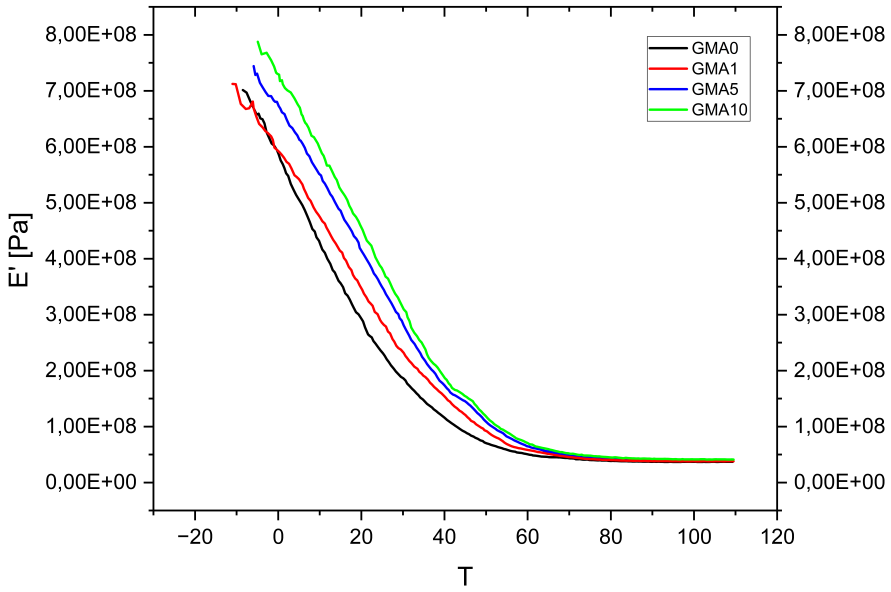

Figure 3.6: Storage modulus E'

Formulation	E'_{ult} [MPa]	v_c [mol/m^3]
GMA0	37.03	3986
GMA1	37.88	4054
GMA5	39.22	4150
GMA10	41.36	4334

Table 3.3: Ultimate storage modulus E'_{ult} and volumetric crosslink density v_c

The results for crosslink density align with the expectations, since adding GMA to the reagent mixture increases the density of functional groups, given that GMA is a much smaller molecule compared to AESO [21]. Adding 10% GMA thus results in an 8.7% increase in crosslink density, a small but measurable difference.

3.4. Rheology

The results of the rheological analysis are displayed in *Figure 3.7* and the relevant values of viscosity η for each formulation (around γ'=10 s^{-1}, well within the plateau), are summarized in *Table 3.4*.

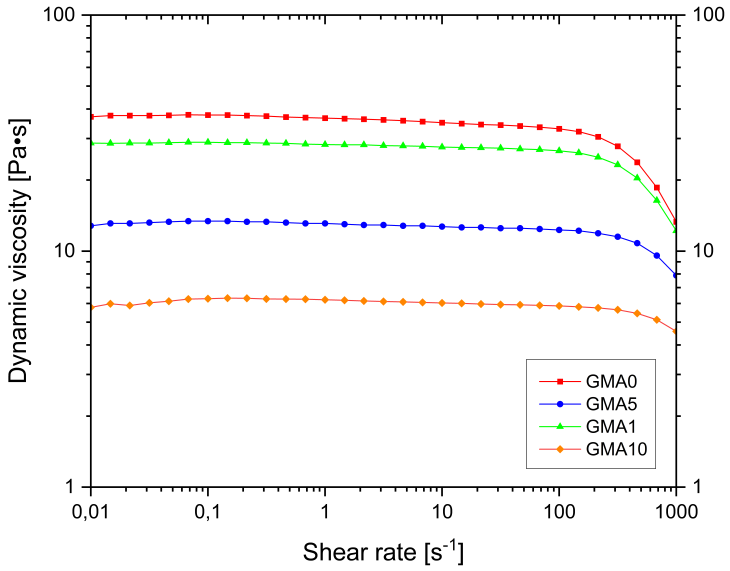

Figure 3.7: Rheology results

Formulation	η at γ'=$10s^{-1}$ [Pa•s]
GMA0	34.7
GMA1	27.6
GMA5	12.7
GMA10	6.03

Table 3.4: Dynamic viscosity at values of shear rate relevant for 3D printing

The results indicate, according to the literature regarding resins for the purpose of 3D printing, that only the formulation with the most dilutant, GMA10, would be definitely suitable for such purpose, while the second highest, GMA5, is still close enough to the desirable range of η=0.2-10 Pa*s to warrant further investigation.

For the sake of completeness, the other two formulations, GMA1 and GMA0, also underwent 3D printing trials. As discussed in *Section 3.8*, most of those attempts succeeded against expectations. This indicates that viscosity might be a less important factor than reported for certain printed structures, especially those mostly composed of narrower component sections, in which the resin flowing in to fill the gaps left by the receding latest layer have enough time to be flooded even by a more viscous, and thus slower flowing resin. The parts tested in this work, such as honeycomb and gyroid structures, fall within this category.

3.5. Photorheology

The results of the photorheological analysis are summarized in *Figure 3.8*.

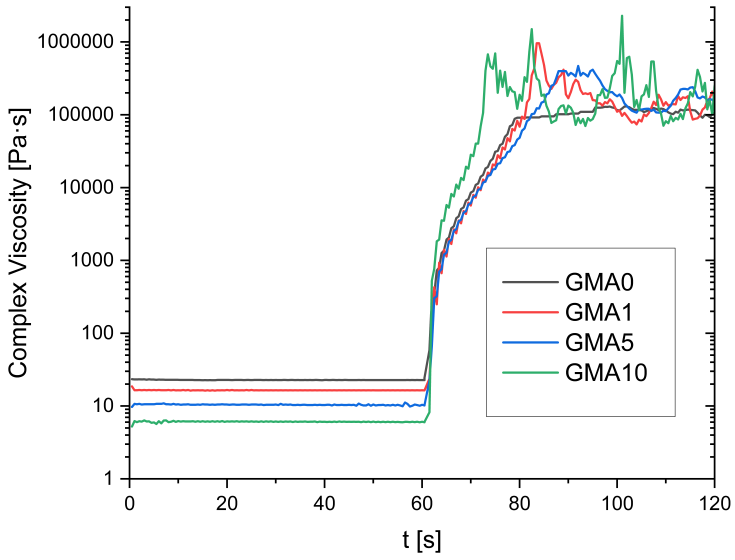

Figure 3.8: Photorheology results

The first 60 seconds of readings, gathered with the UV light not yet turned on, correspond to the equivalent results of the rheological analysis, corroborating the conclusion that the viscosity of the reagent mixture decreases alongside the concentration of GMA.

At t=60 s, the UV lamp is activated and the polymer starts reticulating, reaching the gelation point at t'=3-4 s (t' being defined as t-60 s, or the time elapsed since the light was turned on). This property shows no correlation to the GMA content across all trials, indicating that such parameter has little bearing on the formation of the gel phase during polymerization.

The three formulations with the lower GMA content exhibit remarkably similar behavior in μ(t'), while the GMA10 formulation hardens significantly faster than the other three. This indicates that, in case GMA10 were used to manufacture goods, it would require significantly less exposure to UV light before it can exist as a free standing film or self supporting body, while the lower concentrations all take comparably longer to become stable.

3.6. Swelling behavior

The analysis of the development of the swelling of the material in water, ethanol and acetonitrile was conducted in order to analyze the feasibility of various techniques for the inclusion of a fluorescent probe by immersion in solution. GMA10 was used as a model sample for the solvent selection process, as the swelling behavior of all formulations is rather similar in behavior, if different in its extent. *Figure 3.9* shows the increase in mass (as a percentage of initial mass over time) in each solvent.

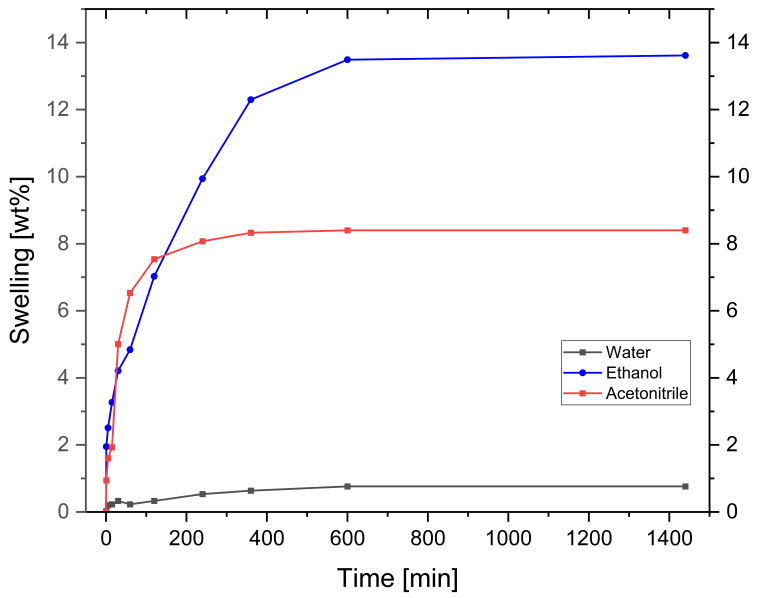

Figure 3.9: Swelling of GMA0 in water, acetonitrile and ethanol

As expected for a non-hydrophilic polymer, the swelling in water is negligible, plateauing around 0.8%. On the opposite end, swelling in ethanol is significant, reaching a plateau between 10 and 24 hours of immersion, with a value of around 13.6% for the GMA10 formulation. Furthermore, as the solvent evaporated from the material after being taken out of the solvent, it started visibly becoming more brittle, then cracking over the course of several hours. This implies that ethanol is most likely unsuited to carry out the inclusion of the probe. The acetonitrile trial was more successful, showing both a lower (albeit still relevant) degree of swelling, at around 8.6%, and most importantly no cracking or signs of losing cohesion as the solvent evaporated. The evaporation of the solvent was conducted both in slow

conditions, by allowing it to dissipate in a closed vial over a period of several days, and fast conditions, in open air under a fume hood assuring the fastest possible drying. Either trial resulted in the material returning to its starting weight without losing structural integrity.

All formulations were then individually tested to find the extent of at the plateau and the time required to reach it. *Figure 3.10* displays the development of the swelling of each matrix with similar methodology as the former figure, and the results are summarized in *Table 3.5*. Both the degree of swelling and the time required to reach the plateau appear to inversely correlate with GMA content, GMA10 being both the fastest and least swelled by the end of the experiment.

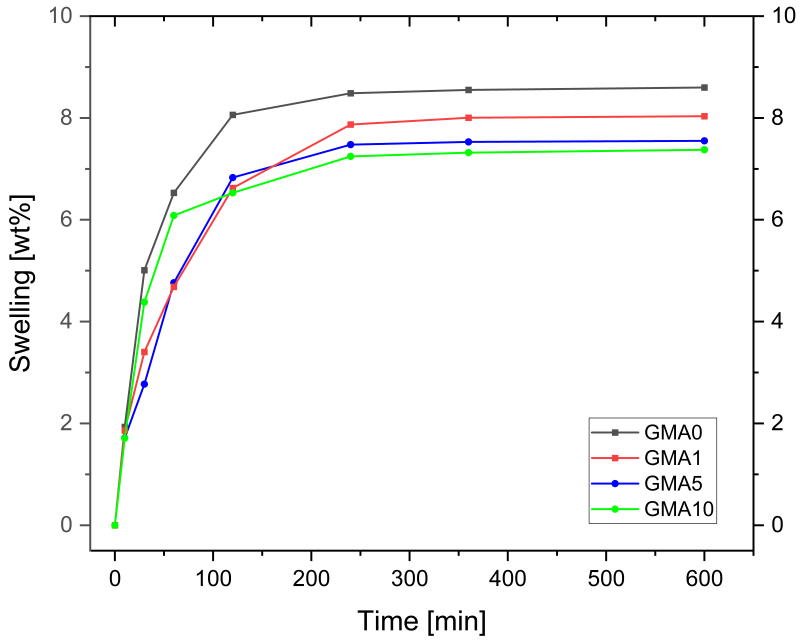

Figure 3.10: Swelling in acetonitrile

Formulation	Swelling [wt%]	$t_{plateau}$ [h]
GMA0	8.60%	8
GMA1	8.04%	8
GMA5	7.55%	6
GMA10	7.37%	6

Table 3.5. Time to plateau and extent of ultimate swelling

Given these results, and the fact that the probe selected for the study is soluble in organic compounds, acetonitrile was selected as a solvent for all solutions containing the probe, both for testing the probe in solution by itself and doping the polymer matrices.

The behavior of the matrix when immersed in a solvent also informed the decision to choose a thickness of 0.8 mm described in *Section 2.2.6*, since smaller dimensions cause the material to warp and bend more intensely, often resulting in a cupped strip. Given the small amount of residual unreacted monomer remaining in the matrix (around 1%), this is rather unlikely to be caused by the leaching of said monomer, but rather by a differential rate of curing between the top layer of the polymer and the bottom one, as the latter receives a significantly lower degree of exposure compared to the former. This assumption is also corroborated by the 3D printed samples showing a lesser degree of warping when exposed to organic solvents, as the layer being exposed to irradiation at a single time is only 25 μm thick.

This was confirmed by way of weighting the residue leftover in solution after immersion. *Table 3.5* displays the extent of residual unreacted monomer for each

formulation, both in samples crosslinked under a UV lamp and 3D printed, expressed as a percentage of starting weight. Naive observation of the samples cured under UV light indicates that such samples are slightly tacky, unlike the 3D printed ones.

Formulation	UV lamp	3D print
GMA0	1.352%	0.147%
GMA1	1.483%	0.128%
GMA5	1.052%	0.104%
GMA10	0.914%	0.116%

Table 3.5. Residue content of extracts

Trials were attempted with samples of varying thickness, and results show that this property doesn't display a significant correlation with the content of residue. This indicates that extraction via solvent is indicative of how much monomer is left unreacted in the finished product.

Furthermore, the amount of unreacted material shows an inverse correlation with GMA content. This is caused by the fact that this compound is more reactive than AESO, and thus more likely to reticulate at equal exposure time. As expected by the naive observation of the tackiness of the samples, the 3D printed samples have a significantly lower residue content.

3.7. Inclusion of the pH-sensitive probe in the matrix

As discussed in *Section 2.2.8*, after determining that the synthesized probe functioned correctly in solution, the fluorimeter readings for the swelled probe resulted out of

scale by several orders of magnitude, indicating that the polymer matrix possessed some degree of intrinsic fluorescence, which interfered with the weaker signal provided by the probe.

This resulted in the necessity to dramatically increase the concentration of the probe in order to render its emission strong enough to overcome the intrinsic fluorescence of the matrix.

One example of the fluorescence spectrum of the probe when included in the matrix is shown in *Figure 3.11.* The peak of each curve (corresponding to a wavelength of around 500 nm) corresponds to the *emission intensity* used in the following plots.

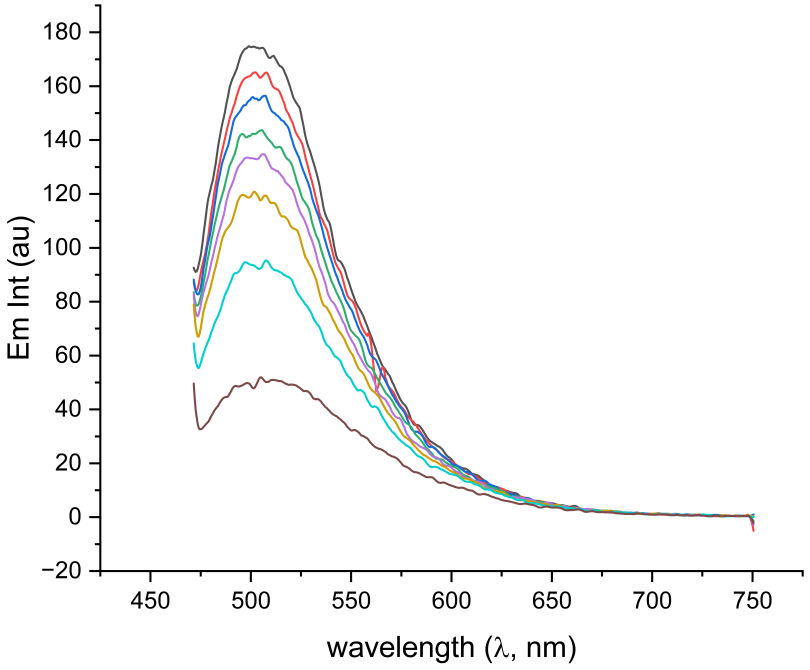

Figure 3.11: Fluorescent emission spectra of the matrix-probe complex

Figure 3.12 displays the behavior of the GMA0 matrices, following the inclusion of the probe, when immersed in a solvent, followed by the addition of TFA.

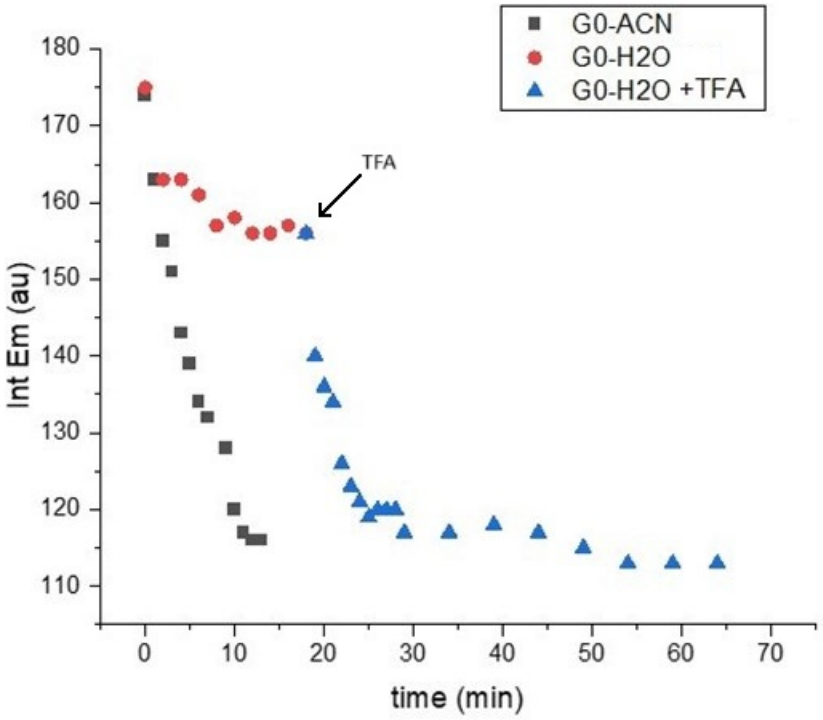

Figure 3.12: Variation of the maximum emission intensity of the GMA0-probe matrix over time when immersed in acetonitrile, water and after addition of 50μL of trifluoroacetic acid

The red data points indicate the intrinsic fluorescence of the matrix when immersed in water, which displays a small but not insignificant decrease in intensity over time. When equilibrium was reached, 50 μL of TFA were added to the cuvette, which drastically decreased the intensity of the signal, indicating that the phenomenon causing the fluorescence is pH-sensitive.

The black data points indicate the development of the intensity in acetonitrile,

which appears to be a rapid and drastic decrease, reaching a plateau around 12 minutes of immersion. Given the faster and more intense reaction to the organic solvent, as well as the reaction to the addition of acid, the process appears to be caused by a combination of the swelling caused by immersion, and at the same time by the protonation carried out by the acid. These results could be explained by the fact that TICT Donor-Acceptor systems, such as naphthalimide, experiment a decrease in their emission intensity when free volume increases in their microenvironment (because of higher free rotation around the 4C-N bond of the naphthalimide molecule). In our system, both swelling of the matrix and protonation of the inner functional groups (both hydroxyl and epoxy groups) will cause an expansion of the crosslinked network [22].

Similar results for the reaction to acids were obtained in dry conditions, by adding 50 μL of acetic acid to the bottom of the cuvette containing the matrix and no solvent, and leaving it to evaporate, as described by *Figure 3.13*. The timescale for vapor doesn't appear to be significantly different from the solvent trials.

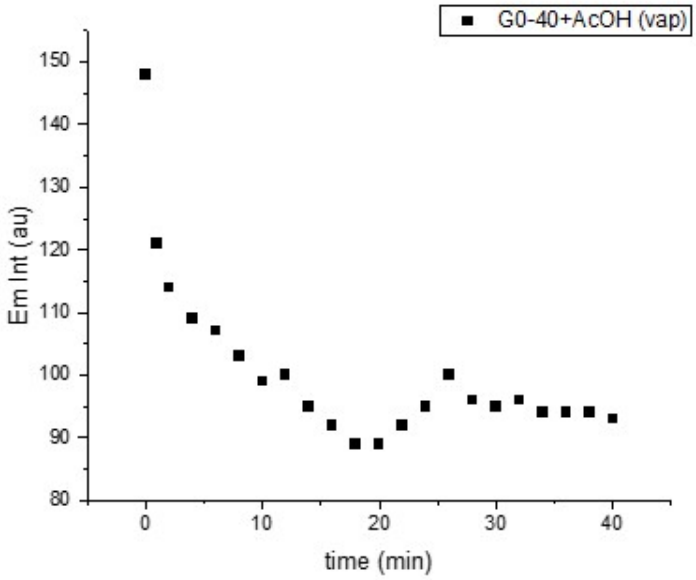

Figure 3.13: dry GMA0 reacting to AcOH vapors

Similar GMA0 samples were also analyzed in pentane and ethanol, both with the addition of TFA, represented in *Figures 3.14* and *3.15*.

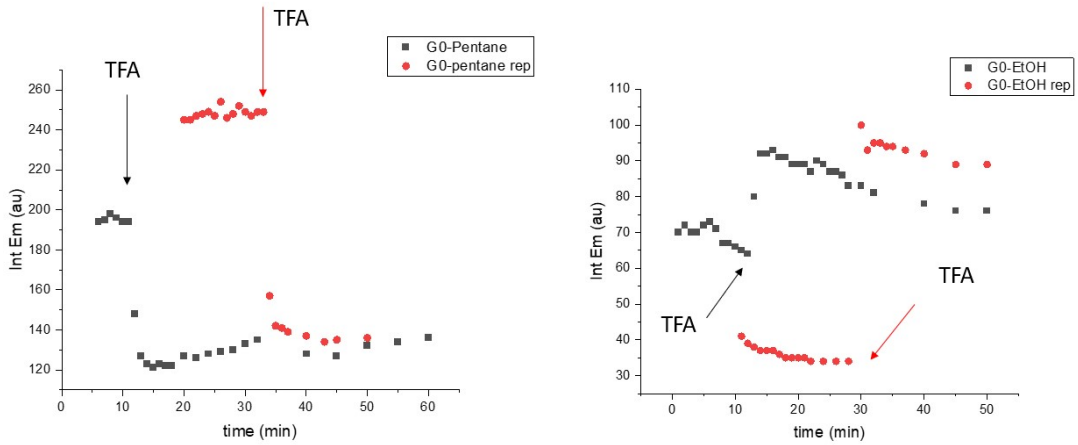

Figure 3.14 and 3.15: GMA0 in pentane and ethanol with TFA additions

The behavior in pentane appears similar to that in acetonitrile, with an initial decrease in intensity of the signal down to a first plateau, and a second rapid decrease when TFA was added. Although not readily apparent in these plots, the addition of TFA causes a dynamic decrease in intensity rather than an instantaneous one (more visible in the former plot, with immersion in water), indicating that the behavior is not purely superficial, and that the acid is able to diffuse into the matrix. On the other hand, addition of acid in ethanol solution appears to increase the relative intensity of the signal. This effect has been consistently reproducible for GMA0 and it didn't occur in GMA10 experiments. The effect isn't likely to be caused by the higher polarity of ethanol, since water causes effects similar to those of other solvents.

GMA10 samples were also analyzed under immersion in water, pentane, acetonitrile and ethanol, followed by the addition of TFA, and the results summarized in *Figures 3.16* and *Table 3.6*.

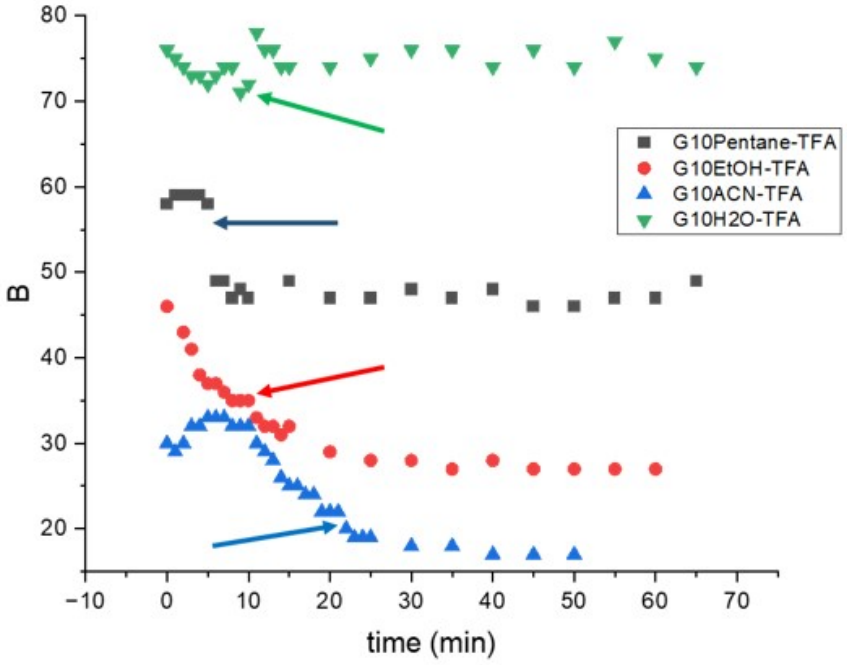

Figure 3.16: GMA10 in pentane, ethanol, acetonitrile and water, before and after the addition of TFA

Solvent	$\%loss_{init}$	$t_{plateau}$	$\%loss_{TFA}$	$t_{plat,TFA}$
Pentane	-	-	16	1
Ethanol	24	8	18	6
Acetonitrile	33	10	23	9
Water	-	-	-	-

Table 3.6: Loss of fluorescence and time to plateau after immersion in solvent and addition of TFA

The table highlights the initial loss of fluorescence associated with swelling, the time needed to reach the plateau, the second loss in intensity caused by the addition

of acid and the time to the latter plateau. Unlike GMA0, GMA10 doesn't exhibit a significant loss of fluorescence in water, even when exposed to acid, possibly due to the more densely crosslinked material, as well as having the expected behavior in pentane, unlike GMA0. Acetonitrile and ethanol cause effects similar to those on GMA0, with acetonitrile having a stronger effect both before and after the addition of TFA.

Overall, the probe appears to behave contrary to expectations. The swelling of the material, which is significant in all the organic solvents analyzed in this work, causes in all cases a decrease in the intensity of the fluorescent emission by the probe. This is likely to be caused by the swelling of the material leading to an increase in the free volume of the matrix, which in turn decreases the intensity of the emission. Similarly, the protonation of the matrix caused by the addition of acid causes a further lowering of the signal. The effect of protonation was demonstrated both in solution with the addition of acid, and dry conditions with exposure to acid vapors.

3.8. MSLA 3D printing

The first printed samples were strips of varying thickness, with the same dimensions as those described in *Section 2.2.6*, pictured in *Figure 3.17*. The strips were used to determine what thickness was sufficient to achieve sufficient stability for immersion in acetonitrile, to avoid warping and cupping of the material. Printing increasingly thinner strips, starting at 1 mm, indicated that a range of 0.7-0.8 mm is sufficient to avoid losing structural soundness of the material, while retaining deformability and using as little material as possible.

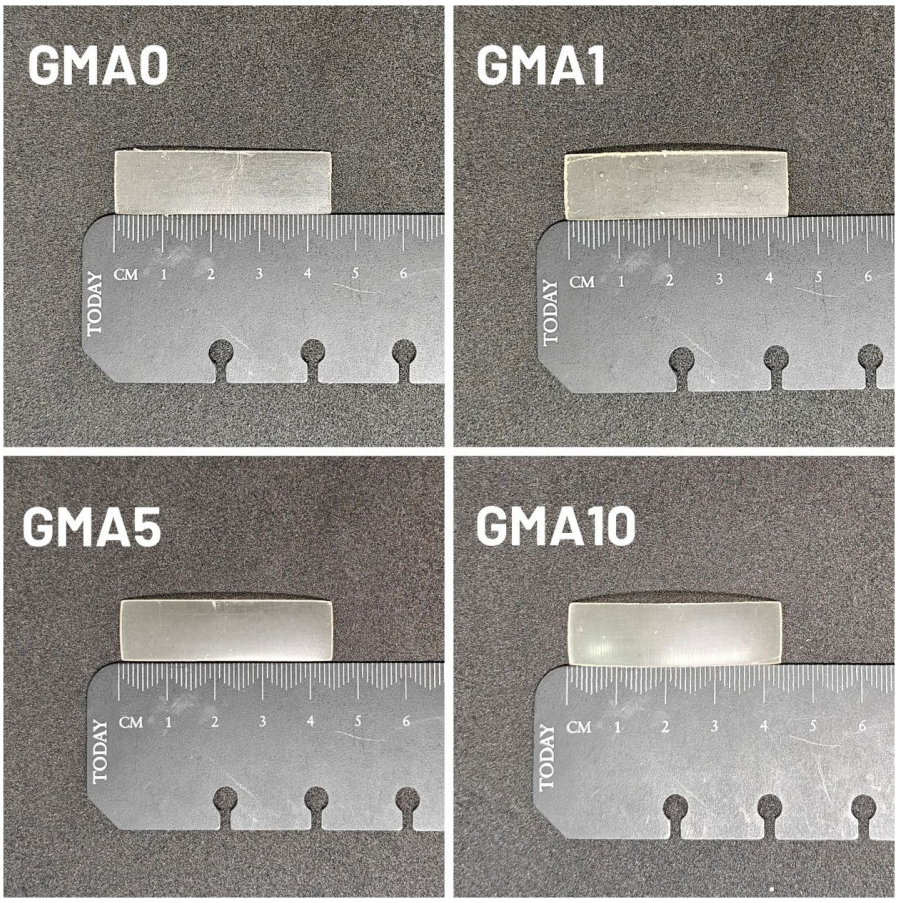

Figure 3.17: 3D printed strips

Against expectations from the rheological study of the resin, the printing of all formulations was successful, including the GMA0 and GMA1, whose viscosity is considered too high for a successful print according to relevant literature.

The first of the complex structures being studied was a hollow honeycomb, chosen for being a remarkably stable structure, with a better ability to disperse longitudinal force than a square mesh, while using much less material than a solid body due to being hollow and *Figure 3.18* displays the final product for each formulation.

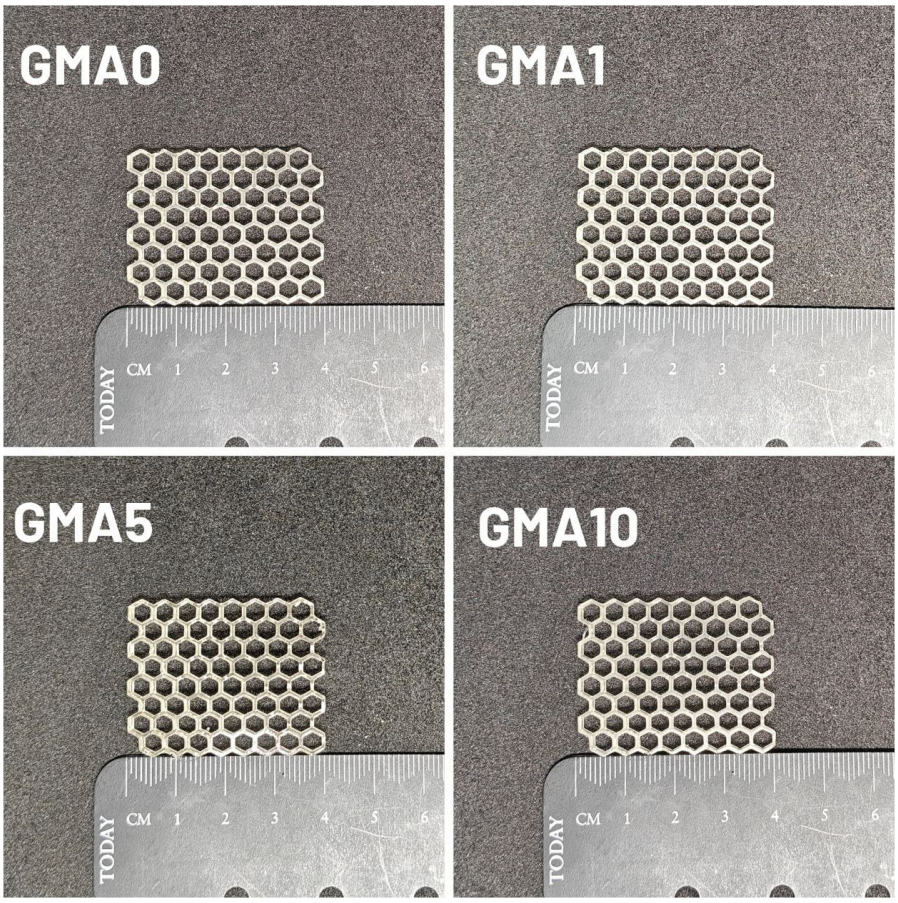

Figure 3.18: 3D printed honeycomb meshes

As can be seen in the figure, all formulations were successfully printed, and none of them displayed the hallmarks of poor printing, such as pitting or layer misalignment. These prints are the simplest of the complex structures considered in this work, as they do not contain voids or overhangs, which are common points of failure for most 3D printed parts.

In order to further test such characteristics, the *periodic minimal surface solids* described in *Section 2.2.8.* were printed. Such shapes are good indicators of the per-

formance of a resin as they are relatively thin and contain many voids and overhangs, which are useful to test the limits of the material.

The printing of Fisher-Koch S structures, depicted in *Figure 3.19* succeeded for all formulations, with near perfect layering and precise edges even from the two more viscous mixtures, GMA0 and GMA1.

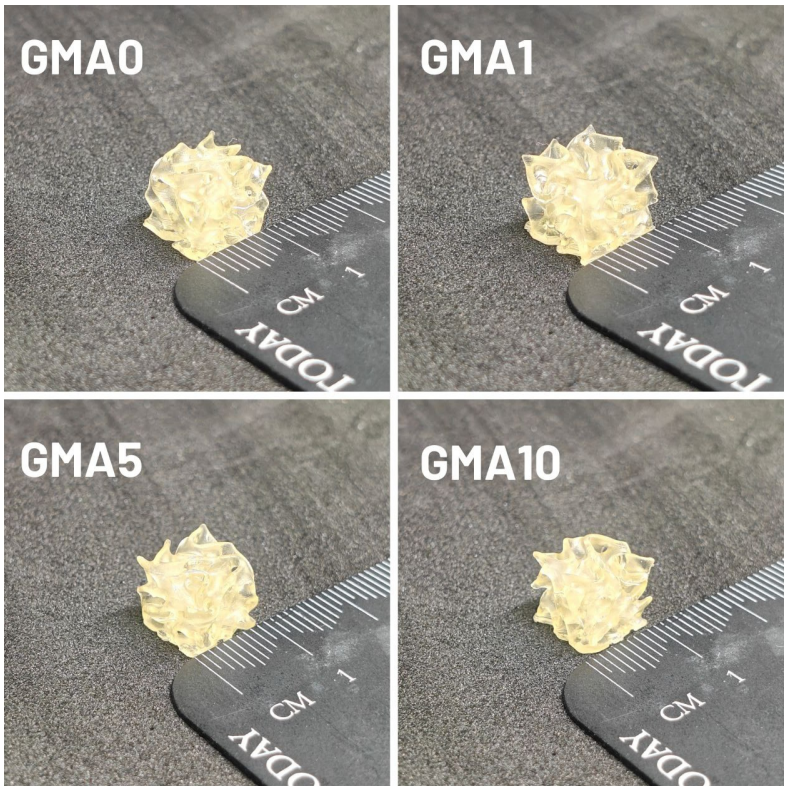

Figure 3.19: 3D printed Fisher-Koch S structures

Schoen F-RD structures, depicted in *Figure 3.20*, proved to be the most challenging, with large unsupported empty spaces and steep inclines, as well as sharp corners caused by the live edge of the unit cell causing a combination of poor layering and the formation of voids. Overall, the GMA0 and GMA1 tended to fail towards the

middle of the large space inside the cell, causing the entire print to collapse. GMA5 and GMA10, on the other hand, demonstrated a high degree of reliability with successes across all attempted prints. GMA10 specifically resulted in a visibly sharper and clearer artifact.

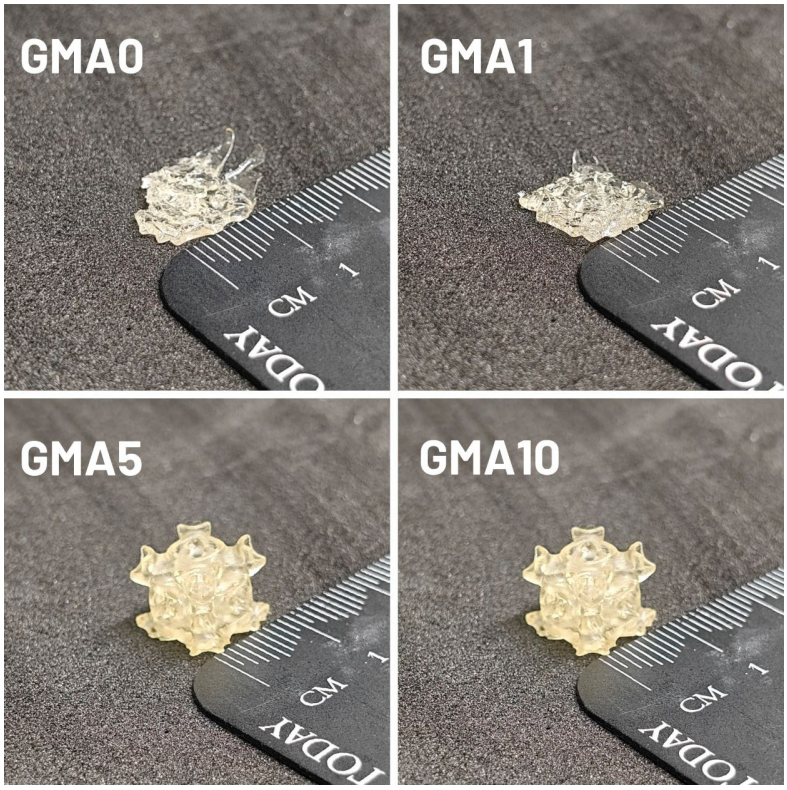

Figure 3.20: 3D printed Schoen F-RD structures

Lastly, the printing of the gyroid structure achieved mixed success. Pure AESO (GMA0) couldn't consistently render the structure, even by varying the printing parameters significantly, possibly due to the extremely thin supports, in the range of 0.2 mm. The two best performing formulations of GMA5 and GMA10 obtained a solid, structurally sound final product, while GMA1 resulted in a successful print

with some defects, such as the thinnest points breaking during normal handling. These problems were limited to the edges of the print, which are thinner than the bulk of the structure since the printed sample constitutes a single cell of a repeating structure.

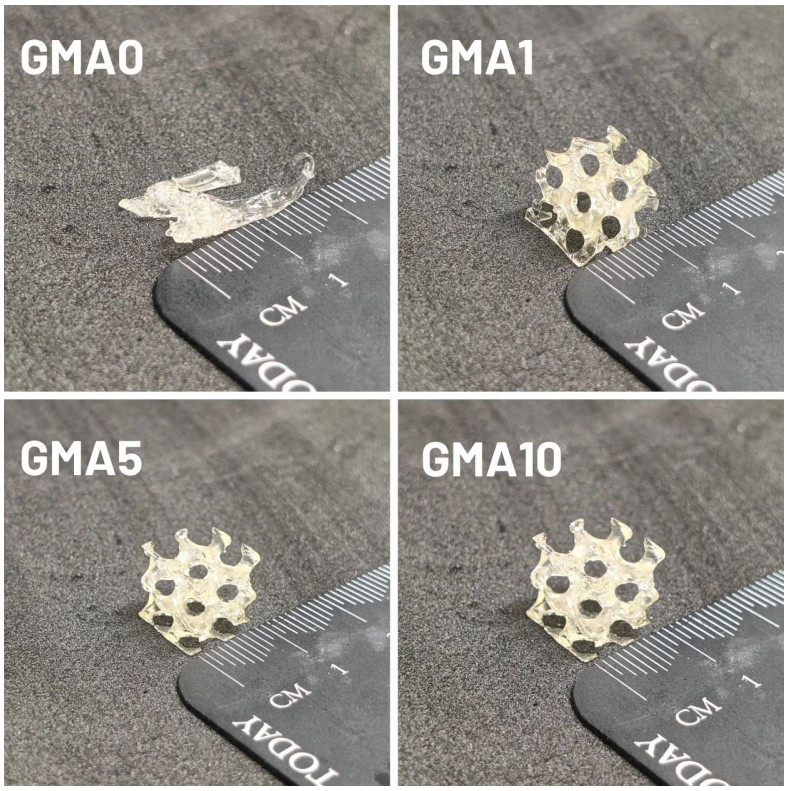

Figure 3.21: 3D printed gyroid

Finally, *Table 3.7* summarizes which formulations succeeded at printing each structure:

Structure	GMA0	GMA1	GMA5	GMA10
Strip	X	X	X	X
Honeycomb mesh	X	X	X	X
Fisher-Koch S	X	X	X	X
Schoen F-RD			X	X
Gyroid		X	X	X

Table 3.7: Successful prints marked for each formulation

Overall, every formulation demonstrated to be printable to some degree, with every formulation succeeding at rendering simple geometries as well as more complex structures such as meshes or simple minimal surface solids. GMA5 and GMA10 further demonstrated the ability to print more complex features such as sharp edges, voids and overhangs without defects.

4. Conclusions

The present work aimed at investigating the properties of an AESO-GMA photopolymer matrix, starting from its characterization, onto the possibility of surface functionalization and 3D printing.

On the count of the polymerization process, the characterization of the material is sufficient to state that the polymer is suited for the creation of solid artifacts at any concentration of GMA, with a higher content providing better and faster crosslinking, as well as a sturdier, less brittle matrix. A similar effect is observed on the crosslink density of the final material. On the other hand, a lower concentration of GMA means that more of the final product would be sourced from bio-based reagents. All formulations display a suitable reaction rate for the production of films via conventional means of photopolymerization. GMA content appears to have a slight, but not insignificant bearing on the thermal characteristics of the material, as well as its dynamic-mechanical properties.

The surface treatment of the matrices has proven challenging due to the intrinsic fluorescence of the material, which is strong enough to interfere with the effect of the probe selected for this work. Due to such effect, attenuation of the fluorimeter signal and a significant increase of the concentration of the probe solution were needed in

order to record the behavior of the matrix-probe complex when exposed to solvents and acids, which renders the measurement overall less reliable. The surface treatment trials for AESO based matrices carried so far can thusly be considered as preliminary, given the conflict between probes and matrices.

Regarding the prospect of 3D printing, all but the highest concentrations of GMA lay the resins outside of the range of viscosity conventionally considered suitable for such processes, but the trials have exceeded expectations. All formulations have been proven to be reliably able to be rendered into simple geometries, such as films or strips, as well as more cross-sectionally complex structures, such as square or honeycomb meshes. Structures with complex patterns in all axes, such as gyroids or other objects with remarkably complex to print parts like voids or overhangs, have been printed with the higher-concentration formulations of GMA5 and GMA10. These trials indicate that AESO-based resins provide a reliable foundation for the 3D printing of bio-based artifacts.

Bibliography

[1] Paulien Harmsen, Martijn Hackmann, and Harriëtte Bos. Green building blocks for bio-based plastics. *Biofuels, Bioproducts and Biorefining*, 8, 05 2014.

[2] T. Pirman, M. Ocepek, and B. Likozar. Radical polymerization of acrylates, methacrylates, and styrene: Biobased approaches, mechanism, kinetics, secondary reactions, and modeling. *Industrial & Engineering Chemistry Research*, 60(26):9347–9367, 2021.

[3] Elisa Caussin, Christian Moussally, Stéphane Le Goff, Timothy Fasham, Max Troizier-Cheyne, Laurent Tapie, Elisabeth Dursun, Jean-Pierre Attal, and Philippe François. Vat photopolymerization 3d printing: A comprehensive review of actual popular technologies. *Materials*, 17(4), 2024.

[4] Marek Pagac, Jiri Hajnys, Quoc-Phu Ma, Lukas Jancar, Jan Jansa, Petr Štefek, and Jakub Mesicek. A review of vat photopolymerization technology: Materials, applications, challenges, and future trends of 3d printing. *Polymers*, 13:598, 02 2021.

[5] Ian Gibson, David Rosen, and Brent Stucker. *Additive manufacturing technolo-*

gies: 3D printing, rapid prototyping, and direct digital manufacturing, second edition. Additive Manufacturing Technologies, 01 2015.

[6] Lindani Ncube, Albert Ude, Enoch Ogunmuyiwa, Rozli Zulkifli, and Isaac Beas. An overview of plastic waste generation and management in food packaging industries. *Recycling*, 6:12, 02 2021.

[7] Lucy-Caterine Daza-Gómez, Xochitl-Andrea Hernández-Contreras, Lisbet Martín, and David Díaz. *Recent Advances in Plastic Degradation and Conversion by Photocatalysis*, pages 151–193. American Chemical Society, 11 2024.

[8] Jyoti Rani, Vibhuti Gulia, Sahil Dhull, Deepak Beniwal, and Deepali. *Active Packaging for Convenience Foods: Enhancing Quality and Sustainability*, pages 455–482. Springer, 01 2025.

[9] Sandra Medel, Enrique Martínez-Campos, David Acitores, Evgenia Vassileva-Tonkova, Ivo Grabchev, and Paula Bosch. Synthesis and spectroscopic properties of a new fluorescent acridine hyperbranched polymer: Applications to acid sensing and as antimicrobial agent. *European Polymer Journal*, 102:19–29, 2018.

[10] Ana Dotan. 15 - biobased thermosets. In Hanna Dodiuk and Sidney H. Goodman, editors, *Handbook of Thermoset Plastics (Third Edition)*, pages 577–622. William Andrew Publishing, Boston, third edition edition, 2014.

[11] Chunsheng Cheng, Zhenyun Wei, Xu Ming, Jie Hu, and Rong Kong. Study on reaction mechanism and process safety for epoxidation. *ACS Omega*, 8, 11 2023.

[12] Max Schmallegger, Hansjörg Grützmacher, and Georg Gescheidt. Bis(acyl)phosphine oxides as stoichiometric photo-reductants for copper nanoparticle synthesis: Efficiency and kinetics. *ChemPhotoChem*, 6, 09 2022.

[13] Dapawan Kunwong, Natthawadee Sumanochitraporn, and Supranee Kaewpirom. Curing behavior of a uv-curable coating based on urethane acrylate oligomer: The influence of reactive monomers. *Songklanakarin Journal of Science and Technology*, 33, 04 2011.

[14] Matteo Bergoglio, Ziba Najmi, Andrea Cochis, Marta Miola, Enrica Vernè, and Marco Sangermano. Uv-cured bio-based acrylated soybean oil scaffold reinforced with bioactive glasses. *Polymers*, 15:4089, 10 2023.

[15] Jin Zhou, Canliang Fang, Chang Tianjun, Xiangjun Liu, and Dihua Shangguan. A ph sensitive ratiometric fluorophore and its application for monitoring the intracellular and extracellular phs simultaneously. *J. Mater. Chem. B*, 1:661–667, 01 2013.

[16] Jiaxuan Wang, Chenyi Qian, Binbin Yu, Fengrui Zhang, Ruixin Ma, Junye Shi, and Jiangping Chen. Design and optimization of additive manufactured fischer-koch-structured heat exchanger for enhanced heat transfer efficiency. *International Communications in Heat and Mass Transfer*, 159:108078, 12 2024.

[17] Andrew Fogden. A systematic method for parametrising periodic minimal surfaces : the f-rd surface. *http://dx.doi.org/10.1051/jp1:1992138*, 2, 03 1992.

[18] Adam Khan, Winowlin J T, Gyasi Ebenezer, R. Narendran, R. Bharathvaj, and

K. Amuthan. Studies on design and analysis of gyroid structure using additive manufacturing process. *Interactions*, 245, 08 2024.

[19] Massimo Benaglia, Angelo Alberti, Loris Giorgini, Francesco Magnoni, and Silvia Tozzi. Poly(glycidyl methacrylate): A highly versatile polymeric building block for post-polymerization modifications. *Polym. Chem.*, 4:124–132, 2012.

[20] Cong-Cong Huang, Ming-Xuan Du, Bao-Qing Zhang, and Chen-Yang Liu. Glass transition temperatures of copolymers: Molecular origins of deviation from the linear relation. *Macromolecules*, 55(8), 2022.

[21] Jinrui Huang, Pan Fu, Wenbin Li, Laihui Xiao, Jie Chen, and Xiaoan Nie. Influence of crosslinking density on the mechanical and thermal properties of plant oil-based epoxy resin. *RSC Advances*, 12, 2022.

[22] Nikolai Georgiev, Ventsislav Bakov, Kameliya Anichina, and Vladimir Bojinov. Fluorescent probes as a tool in diagnostic and drug delivery systems. *Pharmaceuticals*, 16:381, 03 2023.